The Portuguese Large Wildfire Spread Database (PT-FireSprd)

Akli Benali[1], Nuno Guiomar[2], Hugo Gonçalves[3,4], Bernardo Mota[5], Fábio Silva[3,4], Paulo M. Fernandes[6], Carlos Mota[3,4], Alexandre Penha[4], João Santos[3,4], José M.C. Pereira[1,7], Ana C.L. Sá[1]

[1]Centro de Estudos Florestais, Instituto Superior de Agronomia, Universidade de Lisboa, Tapada da Ajuda, 1349-017 Lisboa, Portugal
[2]MED - Mediterranean Institute for Agriculture, Environment and Development; CHANGE - Global Change and Sustainability; EaRSLab - Earth Remote Sensing Laboratory Institute; IIFA - Institute for Advanced Studies and Research; University of Évora, 7006-554 Évora, Portugal
[3]Força Especial de Proteção Civil, 2080-221 Almeirim, Portugal
[4]Autoridade Nacional de Emergência e Proteção Civil, 2799-51 Carnaxide, Portugal
[5]National Physical Laboratory (NPL), Climate Earth Observation (CEO), Hampton Rd. Teddington, TW11 0LW, UK
[6]CITAB - Centro de Investigação e de Tecnologias Agro-Ambientais e Biológicas, Universidade de Trás-os-Montes e Alto Douro, 5001-801 Vila Real, Portugal;
[7]Laboratório Associado TERRA, Tapada da Ajuda, 1349-017 Lisboa, Portugal

Correspondence to: Akli Benali (aklibenali@gmail.com)

Abstract. Wildfire behaviour depends on complex interactions between fuels, topography and weather, over a wide range of scales, being important for fire research and management applications. To allow for a significant progress towards better fire management, the operational and research communities require detailed open data on observed wildfire behaviour. Here, we present the Portuguese Large Wildfire Spread Database (PT-FireSprd) that includes the reconstruction of the spread of 80 large wildfires that occurred in Portugal between 2015 and 2021. It includes a detailed set of fire behaviour descriptors, such as rate-of-spread (ROS), fire growth rate (FGR), and fire radiative energy (FRE). The wildfires were reconstructed by converging evidence from complementary data sources, such as satellite imagery/products, airborne and ground data collected by fire personnel, official fire data and information in external reports. We then implemented a digraph-based algorithm to estimate the fire behaviour descriptors and combined it with MSG-SEVIRI fire radiative power estimates. A total of 1197 ROS and FGR estimates were calculated along with 609 FRE estimates. The extreme fires of 2017 were responsible for the maximum observed values of ROS (8900 m/h) and FGR (4400 ha/h). Combining both descriptors, we describe the fire behaviour distribution using six percentile intervals that can be easily communicated to both research and management communities. Analysis of the database showed that burned extent is mostly determined by FGR rather than by ROS. Finally, we explored a practical example to show how the PT-FireSprd database can be used to study the dynamics of individual wildfires and to build robust case studies for training and capacity building.

The PT-FireSprd is the first open access fire progression and behaviour database in Mediterranean Europe, dramatically expanding the extant information. Updating the PT-FireSprd database will require a continuous joint effort by researchers and fire personnel. PT-FireSprd data are publicly available through https://doi.org/10.5281/zenodo.7495506 (last access: 30th

December 2022) and have a large potential to improve current knowledge on wildfire behaviour and support better decision-making (Benali et al. 2022).

Keywords: fire behaviour; satellite; airborne; ground data; rate of spread; fire radiative energy; graphs; progression

1 Introduction

Wildfire behaviour is broadly defined as the way a free-burning fire ignites, develops and spreads through the landscape (Albini 1984; Rothermel 1972). It depends on complex interactions between fuels, topography and weather, over a wide range of temporal and spatial scales (Santoni et al., 2011; Countryman, 1972). Wildfire behaviour can be described using common metrics such as the spread rate, growth rate, rate of energy release and flame length (Albini 1984). Fire behaviour data is important for fire research and management applications (Finney et al., 2021).

To allow for a significant progress towards better fire management, the operational and research communities require detailed open data on observed wildfire behaviour (Gollner et al., 2015). In this context, systematic mapping of the fire front progression through space and time is critical to address existing needs, particularly of wildfires burning under a wide range of environmental conditions (Storey et al., 2021; Gollner et al., 2015). Compiling quality fire behaviour information is important to develop reliable and well-suited fire spread models and for a much-needed extensive evaluation of fire behaviour predictions, which is paramount to support the decision-making process (Alexander and Cruz, 2013a; Scott and Reinhardt, 2001). This includes planning pre-suppression activities and defining resources dispatch to wildfires, delineating safe and effective fire suppression strategies and tactics during a wildfire, and for early alert and evacuation purposes (Finney et al., 2021). Comprehensive fire progression and behaviour information is also useful to develop burned area/fire perimeter mapping algorithms (Valero et al., 2018), understand fire effects (Collins et al., 2009), fire danger rating (Parisien et al., 2011), fire hazard mapping and risk analysis (Alcasena et al., 2021, Palaiologou et al., 2020), planning and implementation of preventive fuel treatments (Salis et al., 2018), and also to foster robust training of operative personnel and researchers improving their learnings from past wildfires (Alexander and Thomas, 2003). Unfortunately, reliable quality information on the progression and behaviour of wildfires, especially those burning under extreme conditions, is difficult to collect (Gollner et al., 2015).

Fire behaviour data can be collected from laboratory experiments, experimental fires, prescribed fires or wildfires. A large number of laboratory-scale experiments have been made for the development of semi-empirical rate-of-spread (ROS) models (Rothermel 1972; Catchpole et al., 1998). Experimental fires have been set up to collect fireline data, estimate fire behaviour descriptors and develop empirical fire spread models (Forestry Canada Fire Danger Group 1992; Fernandes et al., 2009; Cruz et al., 2015), requiring significant time and resources. Neither laboratory-scale nor experimental fires represent the spatial and temporal variability of environmental conditions under which uncontrolled wildfires most often burn (e.g. Gollner et al., 2015).

Due to the unpredictability of their timing and location, conventional measurements on wildfires are difficult to perform and lead to slow accumulation of data (Alexander & Cruz 2013b). Generally, they are of poor quality or incomplete (Duff et al., 2013), although outstanding reconstruction examples exist (e.g. Wade & Ward 1973; Alexander & Lanoville 1987; Cheney 2010). Dedicated efforts do exist (Vaillant et al., 2014), but wildfire behaviour estimates often result from opportunistic

observations (e.g. Santoni et al., 2011) or post-fire interviews (e.g. Butler and Reynolds, 1997). Some authors have made relevant efforts in compiling a large amount of field observations on wildfire behaviour (Alexander and Cruz, 2006; Cheney et al., 2012), some combined with experimental fire data (Cruz and Alexander, 2013, 2019; Anderson et al., 2015; Cruz et al., 2018, 2021, 2022; Khanmohammadi et al., 2022). An additional limitation lies on the fact that some of the existing fire behaviour datasets are not freely available to the operational and research communities (Gollner et al., 2015).

Remote sensing technology, either through airborne or satellite platforms, can provide relevant data to document wildfire propagation. Manned or unmanned airborne visible and infrared (IR) images have been used to map fire progression (Schag et al., 2021; Storey et al., 2020, 2021; Coen & Riggan 2014; Sharples et al., 2012). Satellite data provide easy-to-use, autonomous, synoptic observations of fire activity worldwide. Recent advances in satellite technology have made available a panoply of open-access imagery and products with capabilities to monitor wildfires over the entire globe. Their characteristics vary in resolution, ranging from high (10-30 m) to low (4-5 km), and frequency of overpass, ranging from 5-15 days to every 15 minutes. To monitor wildfire progression, satellites provide imagery and products that identify where a fire is actively burning at the time of overpass ("thermal anomalies" or "active fire" products). Several authors have used satellite data to map daily fire progression at the country-level (Parks et al., 2014; Veraverbeke et al., 2014, Briones-Herrera et al., 2020; Sá et al., 2017) and at the global scale (Artés et al., 2019; Oom et al., 2016). Some have estimated fire behaviour metrics, such as ROS (Humber et al., 2022; Frantz et al., 2017; Andela et al., 2019). Recently, Chen et al., (2022) improved this research line by using Visible Infrared Imaging Radiometer Suite (VIIRS) data to automatically reconstruct sub-daily fire progression at a higher resolution. Other authors exploited the capabilities of geostationary satellites to monitor wildfires and estimate fire behaviour descriptors (Sifakis et al., 2011; Storey et al., 2021).

The different data sources used to characterise wildfire progression and behaviour have inherent limitations and potentialities. Ground-collected data can be characterised by large uncertainties, particularly when taken by fire personnel whose focus is on suppression and not on data collection (Alexander and Thomas, 2003). In addition, ground-collected data have poor synoptic capability and provide a limited representation of fire behaviour variability. For example, distribution of ROS values for single fire runs are seldom available (Cruz, 2010). Airborne data can provide wider coverage of the fire progression, although, have limited temporal acquisition windows (e.g. USFS National Infrared Operations - NIROPS - provides data once per night) and in some cases require manual digitization of fire perimeters (Stow et al. 2014; Veraverbeke et al., 2014; Storey et al. 2021).

The tradeoff between spatial and temporal resolution of satellite data, as well as the presence of clouds and thick smoke can significantly limit their fire monitoring capability. In addition, the correct location of a wildfire cannot be determined inside a burning pixel whose size varies with viewing geometry and sensor properties (Wolfe et al., 1998). Daily or sub-daily satellite-derived fire progressions can also fail to reflect the influence of extreme conditions in fire behaviour due to the effect of averaging over relatively long periods (Collins et al., 2009).

Considering that all data sources have limitations and provide information for very limited periods, combining different sources is key to capture the spread and behaviour variability of wildfires. The example provided in Figure 1 highlights the potential of combining different data sources to overcome inherent acquisition gaps, particularly in the afternoon, when both field and airborne data overcome the satellite gap, and during dawn, when ground-collected and satellite data complement each other. Note that observation frequencies of ground and airborne data strongly depend on daily fire activity patterns.

(Figure 1 near here)

Systematic multi-source acquisition of wildfire data collection was recently done by Kilinc et al., (2012) and Storey et al., (2020, 2021) for Australia, by Crowley et al., (2019) for Canada (only satellite data) and by Fernandes et al., (2020) at the global scale. The pursuit of this goal requires a monitoring framework and a concerted joint effort between research and operational communities (Stocks et al., 2004; McCaw et al., 2012, Storey et al., 2020, 2021). Additional data on constantly evolving wildfires, accompanied by robust replicable methods, is needed, namely in southern Europe where there is a substantial data gap (Fernandes et al., 2018).

Here, we present the Portuguese Large Wildfire Spread Database (PT-FireSprd), which combines data from multiple sources, using a "convergence of evidence" approach to characterise in detail the progression and behaviour of large wildfires in Portugal. Fire behaviour is described *sensu stricto*, thus analysis of its drivers, namely weather and fuel, and effects is beyond the scope of the current work. The work results from a joint co-creation effort between researchers and fire personnel, integrating data collected from airborne and ground operational resources.

2 Data and Methods

2.1 Overview

We first collected data for all the large wildfires (>100 ha) that occurred in mainland Portugal between 2015 and 2021. Out of 14,973 wildfires that occurred during this period, 793 (about 5%) had an extent larger than 100 ha. These were responsible for almost 1 million hectares burned, of which half occurred in the extreme fire season of 2017. About 90% of the total burned area resulted from the 760 largest wildfires.

Multi-source input data (L0, section 2.2) were collected and only wildfires with good quality data and representative of its spread were kept. Fire progressions were reconstructed from the input data and fire behaviour metrics were estimated. The PT-FireSprd database was then organised in three levels:

- L1: Wildfire progression (section 2.3), representing the spatial and temporal evolution of the wildfire spread (i.e. where and when).

- L2: Wildfire behaviour (section 2.4), including quantitative behaviour descriptors of how a wildfire burned, such as the rate-of-spread (ROS), fire growth rate (FGR), fire radiative energy (FRE), and FRE flux;
- L3: Simplified wildfire behaviour (section 2.5), averaging behaviour descriptors over longer periods that represent relatively homogenous fire runs.

The data from the different levels were composed by a large set of maps that can be useful for several applications and target users. For example, L1 data can be used by fire analysts or researchers to evaluate suppression strategies and understand the fire spread drivers or to evaluate burned area/fire perimeter mapping algorithms. L2 data are useful, for example, to calibrate existing or build better fire spread models, while potential applications of L3 are improving fire danger rating, fire hazard mapping and risk analysis. The overall flow of the data and methods is described in Figure 2.

(Figure 2 near here)

2.2 Input Data (L0)

To reconstruct the wildfire progressions, we used data acquired by satellites, from airborne sources and in the field by fire personnel. Most of these data are currently integrated in a near-real time operational WEB-GIS fire monitoring platform (in Portuguese "FEB Monitorização", hereafter FEBMON) developed in 2018 by the Civil Protection Special Force (FEPC) and the Portuguese National Authority for Emergency and Civil Protection (ANEPC). The data were complemented with official fire data and information from external reports. Table A1 summarizes the different data sources used and their main characteristics.

2.2.1 Satellite data

The Sentinel-2 Multispectral Instrument (MSI) and the Landsat 8/9 Operational Land Imager (OLI) provide images on average every 5 days and every 16 days, respectively, with a spatial resolution ranging between 10 and 60 m. PROBA-V has a low number of spectral bands (4) and provides daily images at 300 m of spatial resolution, and every 5 days with a 100 m spatial resolution. The VIIRS instrument aboard the NPP and NOAA-20 satellites collects data on average twice per day with a resolution of 375 m and 750 m. The Moderate-Resolution Imaging Spectroradiometer (MODIS) is an instrument on board the TERRA and AQUA satellites with spatial resolutions ranging from 250 m to 1000 m, providing on average four daily revisits when combined. Sentinel-3 satellites have onboard the Sea and Land Surface Temperature Radiometer (SLSTR) and the Ocean and Land Color Instrument (OLCI), with spatial resolution ranging between 500 and 1000 m for the former, and 300 m for the latter. Data are acquired on average twice per day, but the OLCI does not retrieve nighttime data.

We used atmospherically corrected (L2) satellite imagery to create false colour composites that could highlight burned areas (low NIR, high SWIR reflectance), active flaming areas (high SWIR and/or TIR reflectance) and unburned vegetation (high

NIR reflectance). Typical false colour composites use bands 12-8A-4 of Sentinel-2, bands 7-2-1 for MODIS and bands 1-2-4 for PROBA-V. Most imagery were downloaded from Sentinel EO Browser (https://apps.sentinel-hub.com/eo-browser/), Worldview (https://worldview.earthdata.nasa.gov/) and VITO-EODATA (https://www.vito-eodata.be/PDF/) which allow easy and fast access to historical L2 data.

To complement the satellite imagery, we used the thermal anomaly products of VIIRS (VNP14IMGML-C1, Schroeder et al., 2014, 2017) and MODIS (MCD14ML-C6, Giglio et al., 2003, 2016), with 375 m and 1 km resolution at nadir, respectively. Data are available at fuoco.geog.umd.edu and FIRMS (https://firms.modaps.eosdis.nasa.gov/). These products allow estimating the approximate location and timing of an active wildfire, and provide an estimate of the fire radiative power (FRP), a proxy of the radiant energy released per time unit, and a proxy for fuel consumption and fireline intensity. In addition, coarse resolution data (~4 km) from the Spinning Enhanced Visible and Infrared Imager (SEVIRI) sensor onboard the Meteosat Second Generation (MSG) geostationary satellite, was used to characterise the temporal evolution of fire activity using FRP estimates every 15 min (Wooster et al., 2015). Data are available at https://landsaf.ipma.pt/en/products/fire-products/frpgrid/. The FRP detections associated with each wildfire were identified using a spatial-temporal nearest distance algorithm. An empirical threshold derived from the analysis of a selected number of wildfires was used to account for the satellite pixel geolocation and temporal reporting uncertainties. The Fire Radiative Energy (FRE) was estimated based on the FRP detections, assuming a constant rate of energy release every 15 min, and then aggregated in 30 min bins (Eq. 1):

$$FRE_i = 0.0009 \times \left(\sum_{k=1}^{2} FRP_k\right), \quad (1)$$

where index i indicates a 30 min bin, index k indicates the 15 min FRP value in MW, and the 0.0009 factor converts the sum into TJ (Pinto et al. 2017).

2.2.2 Airborne data

Some aeroplanes and helicopters that operate during wildfires collect photos and videos. Data are collected during the initial attack (i.e. up to 90 min after the alert) by the heli-brigades of the National Guard (GNR) using their mobile phones, and occasionally, during extended attack. Aeroplanes, operated by FEPC/ANEPC since 2018 (AVRAC), carry visible and thermal cameras that collect photos and videos during extended attack covering the entire active fire perimeter. In addition, helicopters that coordinate aerial suppression also collect photos and videos. Both data sources collect data only during daytime (with a few exceptions), at relatively low altitudes.

Airborne data are systematically uploaded in real-time in FEBMON, providing high quality information regarding the probable location of the fire start, active flaming zones, and specially wildfire progression. It is noteworthy to mention that airborne footage is not synoptic, as different parts of the wildfire (e.g. left flank vs. right flank) are captured at different moments, which depending on the fire extent and operational priorities, can result in large acquisition time lags.

2.2.3 Ground data

The FEBMON system is linked to portable devices that allow collecting georeferenced ground data during wildfires by fire personnel from several entities. Ground-collected data consists of three main types: i) photos and videos; ii) points that identify active flaming combustion, inactive flaming or smouldering or locations requiring mop-up; iii) polygons that delineate an area burned until the time of acquisition (i.e. fire progression).

Besides the data automatically linked to FEBMON, valuable ad-hoc information was used to reconstruct wildfire spread, such as additional photos\videos and post-fire interviews. In sum, data collected by fire personnel in the field provided valuable spatiotemporal information regarding wildfire spread, ignition and/or wildfire re-activation.

2.2.4 Official fire data

The burned area perimeters for the entire country were provided by ICNF (Instituto da Conservação da Natureza e das Florestas), derived from a combination of fieldwork and satellite data (https://geocatalogo.icnf.pt/). Errors in the burned area perimeters were corrected manually using Sentinel-2 or Landsat 8/9 post-fire false colour composites (see section 2.2.1). For a very limited number of very large multi-day wildfires, we used burned areas (resolution of 1.5 m) provided by the Copernicus Emergency Management Service (https://emergency.copernicus.eu/mapping/).

Regarding ignition data, we used the official wildfire start location, typically derived from post-fire investigation (ICNF, https://fogos.icnf.pt/sgif2010/), the ignition location provided by first responders and time of alert (ANEPC). Ignition data have several known issues (Pereira et al., 2011) the most relevant of which, for the purposes of the present study, is the accuracy of its exact location.

Finally, we analysed the official wildfire time logs from ANEPC, which seldom contain useful contextual information on wildfire location at a given date/hour.

2.2.5 Reports of 2017 large wildfires

We used ignition and fire progression data published in reports of the very large wildfires of June 2017, including the Pedrogão Grande wildfire, and of October 2017 (Guerreiro et al., 2017, 2018; Viegas et al., 2019). Regarding Guerreiro et al. (2017, 2018), the primary data sources used to reconstruct the fire progression were satellite imagery, thermal anomaly data and burned area perimeters provided by the Copernicus Emergency Management Service. Reports from ANEPC and the Portuguese Institute for the Sea and the Atmosphere (IPMA), GNR and the Association for the Development and Industrial Aerodynamics (ADAI), were also used to identify fire arrival times and active firelines. Additionally, other data sources allowed the reconstruction of wildfire spread, such as: the official wildfire time log (see 2.2.4), interviews (fire personnel

involved in suppression, local residents), fieldwork to identify the forward fire spread direction, and other relevant data such as photos and videos. The fire spread isochrones were determined through spatial interpolation methods (spline and inverse distance weighting), on high-density point clouds and experts' knowledge.

Viegas et al., (2019) reconstructed the extreme wildfires of October 2017 based on fieldwork, interviews, photos/videos and information contained in the official wildfire time log. Since the fire progression data were not provided by the authors, here we used only very limited information regarding ignition location\time and general fire spread patterns, mostly to complement data provided by Guerreiro et al., (2017, 2018).

Persistent cloud cover hindered the June and October 2017 wildfires progression mapping with satellite data. Nonetheless, given the relevance of these wildfires we decided to include these fire progressions in our database because they represent some of the largest and most extreme wildfires that ever occurred in mainland Portugal.

2.3 Wildfire Progression (L1)

Wildfire progression characterises the spatial and temporal evolution of the area burned in a specific fire event. To reconstruct wildfire progression, we combined the maximum available data from the different sources mentioned above, with the aim of obtaining convergence of evidence. This allowed reducing the limitations and uncertainties of each individual data source and building higher confidence in the derived wildfire progression.

L1 data also contains information regarding the ignition time and location, as well as, flaming zones that correspond to active areas during the wildfire spread. These include spot fires and reactivation/rekindling areas. Combining all the available data, we manually delimited the extent and time of the ignition, fire progression and active flaming zones of each wildfire. The reconstruction was made chronologically, i.e. starting from ignition and ending with the progression prior to wildfire containment. Sentinel-2 and Landsat 8/9 pre-fire images were used to identify areas burned shortly before the wildfire, and post-fire images were used to correct each progression polygon. As an example, Figure 3 shows how different data sources were combined to derive the spread of the Castro Marim (2021) wildfire. All wildfire progressions (L1) were defined as polygons, each with a set of different attributes (explained below).

(Figure 3 near here)

Ignition location was defined as an area (vector polygon), instead of a point, to account for spatial uncertainties and to have a common data typology for the entire database. To define ignition location we used mostly official data, ignition location provided by first responders and initial attack airborne photos. This was complemented with expert knowledge and information from fire personnel. For a small set of wildfires (mostly with nighttime ignitions), we also used satellite active-fire data to map

the approximate ignition location. All ignitions were compared with later fire spread patterns and with the final burned area to reduce errors and guarantee consistency (e.g. ignition was contained in the final burned area). The official time of alert was compared with 15 min MSG-SEVIRI FRP data to confirm the alert time or, in a very few cases, to anticipate the ignition time if energy was released before. MSG-SEVIRI FRP data were also useful to identify (or confirm) the timing of reactivation(s). An example is shown in Figure 3, where the significant release of energy around 11:30, combined with ground data, allowed identifying the location and time of the reactivation zone.

Active flaming zones were mostly derived from ground, airborne data and/or high spatial resolution satellite imagery. Alternatively, they were defined based on visual interpretation of multiple moderate resolution satellite imagery and often combined with active fire data (mostly VIIRS due to its higher spatial resolution). Inconclusive visual interpretations were discarded, as well as active zones that did not lead to any relevant subsequent fire spread. The ignition zone and all active flaming zones were always contained within the subsequent fire spread polygon.

Wildfire progression was represented by a series of consecutive polygons delineating the temporal evolution of the area burned by the wildfire. The number of polygons depended on fire size and data availability. The progression polygons were built using as many data sources as possible, complementing each other in both space and time (see Figure 1). The variety of input data used have different associated uncertainties. When delineating the progression polygons priority was given to input data with higher spatial resolution, free from smoke and cloud contamination, and with the most complete view of the entire active part of the wildfire. Typically, the first priority level data (i.e. highest confidence) were Sentinel-2 and Landsat 8/9 images, and AVRAC aeroplane photos/videos. The second priority level was composed of ground data, VIIRS active-fires, PROBA-V and Sentinel 3 images (both at 300 m resolution) and helicopter photos/videos. The third priority level were images and active-fire data from moderate resolution satellites (MODIS and Sentinel 3). The fourth, and last priority level (i.e. lowest confidence) were composed by FRP data from MSG-SEVIRI and the official wildfire time logs. The data from the large 2017 wildfires reports were handled separately. The progression polygons from Guerreiro et al., (2017, 2018) were deemed as high confidence data and were complemented with data and information from Viegas et al. (2019) and, at times, with satellite data.

A common challenge found in the delineation of the wildfire progression were the uncertainties associated with the correct time an entire progression polygon burned. These uncertainties were present in almost all data sources. For example, a polygon derived by fire operatives on the ground could have stopped burning minutes or hours before data collection. Additionally, satellite active-fire data can depict areas that are hot minutes or hours after the fire front stopped progressing. The strategy to minimize such uncertainties was to use data from multiple sources, seeking convergence of evidence. As an example, a common feature found in the data was substantial fire spread during daytime, followed by very limited nighttime progression. In these cases, first, the nighttime fire progression was delineated using active fire data (mostly VIIRS) and complemented with ground data, when available. Second, satellite and/or airborne imagery acquired during the following morning were used

to perform any necessary adjustments in the nighttime spread polygon(s). FRE estimates of MSG-SEVIRI were also used to identify if any substantial fire activity occurred between VIIRS/MODIS nighttime overpass and daytime imagery (satellite and/or airborne). We assumed that fire activity decreased significantly when the wildfire released less than 0.5 TJ per 30 min period, and anticipated the date/hour of the fire spread polygon accordingly. In smaller wildfires (<500 ha) this threshold was set to 0.1 TJ. Such thresholds were defined empirically (see Discussion section). The entire procedure reduced the uncertainties associated with the definition of the end date/time of the progression polygons. It should be noted that the fire behaviour within the time span of each progression polygon was unknown and, therefore, it was assumed to be free burning at a constant rate (Storey et al., 2021). When data were insufficient to determine when a given area burned, the spread polygon was flagged as "uncertain".

Ignitions/active flaming zones were linked to the resultant spread polygon(s), by assigning a numeric label to a field called "zp_link", providing an explicit connection between both, and allowing to track the source of a given progression polygon. When information was insufficient, for example, the start of the progression polygon was unknown, zp_link was set to "0". After all ignition(s), fire progressions and active flaming zones were defined, each wildfire was divided into burning periods. We assumed that each burning period contained relatively homogeneous fire runs that:

i) were ignited by the same set of ignitions or active flaming zones;
ii) did not exhibit large fire spread direction shifts (less than 45° of variation);
iii) were not impeded by barriers (e.g. previously burned area) and;
iv) did not exhibit significant changes in fire behaviour (e.g. large ROS variation).

Regarding the latter criterion, for example daytime and nighttime runs were usually separated in different burning periods even if criteria (i) to (iii) were fulfilled. By definition, a new active flaming zone always marked the beginning of a new burning period; however, not all burning periods started with an ignition or active flaming zone, since this depended on data availability.

When direct evidence of fire spotting was available (i.e. exact location/timing of the spot fire(s), typically from ground and/or airborne data), if the fire front(s) rapidly (under 1 hour) coalesced with the original fire front, fire progression was merged into a single polygon. In the remaining cases, typically associated with medium distance spotting and/or slow burning fire fronts, the spotting location was defined as a new active flaming zone setting, defining a new burning period. When the exact location/timing of the spot fire was not available, evidence of spotting consisted of observations of non-contiguous burned areas that resulted from the same wildfire. These were typically separated by rivers, lakes and settlements. In these cases, due to lack of data, the polygons separated from the major fire run were defined with zp_link=0 if the distance was larger than 200 m. No fire behaviour descriptors were calculated for these polygons.

The definition of the burning period was always dependent on data availability and, in some cases, was subjective. For the progressions derived using only satellite data, the length of the burning period was mostly determined by the timing of the satellite overpass(es) and FRE's temporal evolution. For the progressions derived from more detailed data, the above-mentioned criteria were easier to fulfil. In a few cases, uncertainties in fire progressions led to slightly overlapping periods. An example is shown in the Results section and implications are addressed in the Discussion section.

After collecting input data for a large number of wildfires, only those with at least one valid progression and ignition/active flaming zone were kept. We eliminated all suspicious cases where uncertainties were large, for example, due to the presence of persistent smoke or clouds in the satellite/airborne images or absence of valid ground data. The L1 wildfire progression database was defined by a set of polygons with attribute fields (details in section 5). The date/hour of each ignition(s), fire spread and active flaming zones (if applicable) were approximated to the nearest 30 min period. Fire progression data from external reports were adapted to the rationale of the fire database described above.

2.4 Wildfire behaviour (L2)

Fire behaviour descriptors were estimated using spatial graphs. A graph is a mathematical structure composed of nodes (N) and edges (E), which connect the nodes (Dale and Fortin, 2010). Based on the fire spread polygons (L1) (Figure 4a), we built a spatial directed graph (or digraph) where each node refers to a spread polygon, and each edge connects two spread polygons (i.e nodes), with a valid link (i.e. zp_link>0). These two nodes burned at different times, one earlier (ti) and the other later (tj). The value of each edge was defined as the time elapsed between two nodes (Δtij) (Figure 4b). A node can have an inward edge (where fire is being transmitted from) and an outward edge (where fire is being transmitted to).

First, the nodes were connected only if the associated fire progression polygons were contiguous, had the same zp_link value and burned at different timings. Second, only the edges corresponding to the shortest elapsed time between two nodes were kept. The digraph allowed to formally structure the connections between fire spread polygons, enabling the calculation of fire behaviour descriptors.

To allow for a better understanding of the methods used, a brief explanation based on the Ourique (2019) wildfire is provided. In Figure 4, the number of the polygons on the left matches the number of nodes on the right. After its start (1), the wildfire spread fast to the south and burned the area delimited by polygon 2 in about 120 min. Fire behaviour changed after the head run, and the left flank became the head and subsequently made a run to the southeast, burning the area represented by polygons 4, 5, 6 and 7, in about 180 min. This fire behaviour change observed at t=120 min determined the definition of two burning periods: one corresponding to the initial head run, the other corresponding to head run from the left flank. The digraph was built with 7 nodes and 6 edges with values ranging between 30min and 120 min.

(Figure 4 near here)

Based on the fire progression (L1) and the corresponding digraph, we calculated the following set of fire behaviour descriptors (L2): forward ROS (m/h), direction of forward spread (° from North), FGR (ha/h), and FRE (TJ). The polygons referring to areas burned shortly before the fire analysed were removed from L2.

ROS was calculated for each node (Nj) with a valid inward edge (Eij) connecting it to a prior node (Ni). By definition, the forward ROS refers to the head of the fire and was calculated considering the longest distance line connecting two consecutive fire progression polygons (i.e. nodes). representing the fastest spread (Storey et al., 2021). The ground distance (Dij) between each pair of polygons was calculated as follows:

- All ground distances between the polygon vertices of Ni and Nj were calculated, using the European Digital Elevation Model (EU-DEM v1.1, https://land.copernicus.eu/imagery-in-situ/eu-dem/eu-dem-v1.1) resampled to 50 m spatial resolution;
- For each vertex of the Nj polygon, only the shortest distance was kept and the corresponding pair of vertices, from Ni and Nj, were stored;
- Dij was defined as the maximum of all shortest distances between vertices.

The ROS was calculated by dividing the distance (Dij) by the time elapsed between the pair of polygons (Δtij) and expressed in m/h. We divided the ROS calculation in two distinct measures:

- Partial ROS (hereafter, ROSp) calculated between two consecutive polygons;
- Mean ROS (hereafter, ROSi), calculated between the ignition (or active flaming front) and a given spread polygon.

The spread direction was calculated using trigonometric rules considering the two above-mentioned vertices between two polygons. The spread direction was calculated both for ROSp and ROSi, where the difference lies only on the origin polygon. FGR was calculated dividing the burned area by each polygon/node (Aj) by the time elapsed between polygons (Δtij) and was expressed in ha/h. An example of the calculation of these fire behaviour descriptors is shown in Figure 5.

(Figure 5 near here)

In addition to the standard fire behaviour descriptors, we also estimated the FRE for each progression polygon. This procedure raised additional challenges. First, MSG-SEVIRI is affected by clouds and smoke, which can hinder the estimation of FRE for some periods of the wildfires, or for their entire duration. Second, due to the coarse resolution of MSG-SEVIRI it was not possible to calculate the FRE for each polygon directly. To circumvent this, FRE was calculated for each 30 min bin from ignition until the date/hour of the last wildfire spread polygon. In parallel, we estimated the area burned in each spread polygon every 30 min, using its start/end dates and assuming a constant FGR. Then, for each 30 min bin, the total FRE was divided by weighting its value by the proportion of area burned in each spread polygon. Finally, for each spread polygon the 30 min FRE estimates were summed only if they covered more than 70% of its duration (Δt_{ij}), to ensure that the total FRE was representative.

We also estimated the FRE flux rate (GJ ha^{-1} h^{-1}) for each spread polygon by dividing the estimated FRE by the corresponding burned area extent and its duration (Δt_{ij}). As FRE is highly dependent on the extent burning in a given time window, the FRE flux rate can provide estimates closer to "instantaneous" values useful for other applications.

2.5 Simplified Wildfire behaviour (L3)

We calculated simplified metrics representing a mean fire behaviour across each burning period. This enables higher-level analysis of the data, but at the cost of losing detail and making simplifications to the calculation of the fire behaviour metrics.

The simplified ROS corresponded to the ROSi estimated for the last spread polygon of a given burning period i.e., the average ROS between the start and the end of each burning period. FGR was defined as the sum of the area burned in the period divided by its duration. The total FRE was calculated considering all energy released by the polygons burning within the burning period, if FRE estimates covered more than 70% of the area burned.

2.6 Quality Control and Quality Assurance (QC/QA)

All L1 to L2, and L2 to L3 processing was done using Matlab scripts complemented with quality controls checks to identify errors in the original L1 data. These included simple checks to incorrect field names, incoherent data format (e.g., date/hour), and consistency on the fire spread structure defined by the digraphs, as for example: i) time elapsed between node was always positive;and ii) every spread polygon with zp_link>0 was always associated with a predecessor valid node (either of "z" or "p" type), among others.

During the processing of L1 data to L2, we did frequent quality checks to identify potential errors, for example, null values of ROS or FGR associated with valid fire spread polygons, fire progression polygons that did not have a known start/end date, or did not have a known link to a preceding fire source (e.g., active flaming zone). In addition, we selected some wildfires, made independent calculations of the ROS and FGR and compared them with those estimated using the Matlab code developed. All

these quality control steps assured that the data produced were reliable and of the best possible quality. The process was iterative, requiring frequent corrections to the L1 data and re-running the quality check.

Finally, for each wildfire, we defined a confidence flag that provides an overall information of the reliability of the estimated progression data. Although directly related to L1, ultimately it should also provide the user an estimate of the confidence associated with L2 and L3. This was defined empirically, based on the uncertainties that arose in the process of building the fire progression polygons and was graded into a 5-level system where 1 refers to the lowest quality and 5 to the highest quality (Table A2).

3 Results

3.1 Overview of the PT-FireSprd database

The PT-FireSprd database contains data for 80 large wildfires that occurred between 2015 and 2021. The individual wildfire burned area extent ranges from 250 to 45,339 ha, with a mean and median area of 5,990 and 1,665 ha, respectively. The 80 wildfires were distributed throughout mainland Portugal, covering a wide range of environmental conditions (Figure 6). The database spans a wide fire behaviour variability both between (e.g. Figure 6A, B, F) and within each wildfire (e.g. Figure 6C, E, D). The total burned area extent of the wildfires contained in the database is around 460,000 ha, which represents about half of the area burned in the 2015-2021 period. On average, progression was reconstructed for 93% of the area burned by the 80 wildfires, leaving 7% deemed "uncertain". Wildfire behaviour descriptors were estimated for 88% of the burned area extent (ca. 400,000 ha). The time elapsed between two consecutive fire progression polygons ranged between 30 min and 14h30m with an average value of 3h15m. The mean duration of the burning periods was around 8h00m, with a standard deviation of 4h50m.

(Figure 6 near here)

A total of 1,197 polygons with ROS and FGR estimates (L2) were derived from the progression data. We excluded very small polygons (<25 ha) from further analysis, resulting in a dataset with 874 observations. Out of the 1,197 polygons, 609 had FRE estimates. Regarding L3 data, ROS and FGR were calculated for 241 burning periods (L3) and total FRE was estimated for 162 burning periods.

Overall, confidence in the database was lower for the earlier years (2015-2016) because input data were mostly from existent satellites. In 2017, the quality increased due to the integration of: i) ground data; and ii) data from 2017 large wildfires reports. From 2018 onwards, the integration of the monitoring aircrafts, the creation of the FEBMON system, and the rapid availability of all the data that flow through it, significantly improved confidence of the derived fire progressions.

The estimated forward ROS displayed a long-tail distribution (Figure 7, in log-scale) with a median value of 341 m/h and average ROS of 746 m/h, representing large variability (std = 1071 m/h, cv = 143%). About 20% of the ROS values were larger than 1,000 m/h and about 9 % were larger than 2,000 m/h. The maximum observed ROS was 8,900 m/h in the Lousã wildfire of October 2017. The FGR distribution was highly skewed towards low values, with median and average values of 40 ha/h and 191 ha/h, respectively (sd = 438 ha/h, cv = 228%). About 10 % of the observations had FGR larger than 500 ha/h and only about 5 % were larger than 1,000 ha/h. The maximum observed FGR was 4,400 ha/h in the Pedrogão Grande wildfire (2017).

(Figure 7 near here)

The ROS distributions of the L2 and L3 datasets were similar. The largest differences were located in the lower and upper tails, where the L3 ROS tends to be smoother due to the averaging procedure done over a longer time span. The FGR distributions for L2 and L3 were also very similar, probably because all the polygon areas within a burning period are summed, and the value does not result from an average. Differences were larger for more complex wildfires, for example with "finger runs" (e.g. areas resulting from rapid propagation in a different direction than the dominant fire front, often related with wind shifts).

We compared the histograms of L2 ROS and FGR for three aggregated confidence levels. The distribution of ROS estimates for wildfires with lower confidence was slightly skewed towards lower values, when compared with higher confidence estimates (Figure B1). The ROS distributions peaked at 200 m/h, 500 m/h and 800 m/h for very low/low, moderate and high/very high confidence, respectively, showing a clear relationship between confidence and estimated ROS. Regarding FGR, very high values above 500 ha/h were prevalent in wildfires with high and very high confidence progressions (Figure B2). Results are similar if data from external reports for the extreme wildfires from June and October of 2017 are not included.

Estimated ROS and FGR were compared and percentiles 25, 50, 75, 90 and 97.5 were calculated separately for each variable (Figure 8). The percentile values were simplified to enable a clear communication of results, especially between researchers and fire personnel. In general, as ROS increases so does the FGR. However, the relationship between ROS and FGR depends on the morphology of the fire perimeter: elongated fast-spreading wildfires had relatively higher ROS and lower FGR (e.g. Figure 6B, C), while more complex burned area perimeters had relatively lower ROS and higher FGR (e.g. a flank run with an extensive active fireline; see Figure 6A and the last polygons of Figures 6E and 6F). The data scatter tends to increase with higher ROS/FGR values, suggesting a progressively larger dependence on the burned area extent/perimeter. Identification of the drivers behind such relationships is beyond the scope of this work. Nevertheless, wildfires at the extreme of the distribution had both very high ROS and FGR values.

(Figure 8 near here)

Burned area extent is a relevant fire behaviour descriptor for researchers and fire management personnel. Analysis shows that the area burned by a wildfire is mostly determined by its FGR (r=0.84) rather than by the speed of the forward spread (r=0.62; Figure 9a,b). The (cor)relations were lower using L2 data. As expected, FRE is highly correlated with burned area extent (r=0.85, Figure 9c). Correlation between ROS and average rate of energy release (TJ/h) is lower (r=0.30, Figure 9d), although, there is a general direct relation between both descriptors.

(Figure 9 near here)

3.2 Case study: The Castro Marim 2021 wildfire

Here, we describe in detail the progression and behaviour of a specific wildfire to show how the PT-FireSprd database can be used, for example, to analyse case studies, which is often done by researchers and fire analysts.

The Castro Marim wildfire burned 5950 ha on the 16th and 17th of August of 2021. Figure 10 shows its reconstructed progression (a) and associated ROS (b). Ignition occurred at nighttime (01:00) and a single run occurred towards SE until approximately 08:30, defined as the first burning period. The mean ROS was 618 m/h, ranging between 321 and 957 m/h (Figure 10c). The estimated FGR for the burning period was 43 ha/h, ranging between 33 and 77 ha/h, and the total FRE was 13 TJ (Figure 10d).

(Figure 10 near here)

Fire progression halted for about 3h until the wildfire reactivated around 11h30. It spread southwards until the head stopped in an agricultural area around 19h30. In this second burning period, fire behaviour was significantly different from the first. The mean ROS was ca. 1,500 m/h, reaching a maximum value of 3,720m/h between 16:30 and 17:30. On average, the fire grew at a rate of 455 ha/h, however, significant variability was observed with values reaching 1,236 ha/h coinciding with the ROS peak. The behaviour in the second burning period was often between percentiles 90 and 97.5. As a consequence of the behaviour exacerbation, the wildfire released around 38 TJ, with peaks of about 9 and 12 TJ observed during the afternoon. The energy flux rate was highest between 16:00 and 16:30, coinciding with an abrupt increase in ROS (Figure 10d).

After the fire head stopped, a secondary head run stopped around 23:00 in a previously burned area (burning period 3). In the follow-up, two left flank runs were observed, one until 02:30 and the other one, resulting from a reactivation, until 06:00, with

decreasing ROS, FGR and FRE. A secondary peak in the energy flux rate was estimated around 0:00, associated with an increase in ROS and FGR.

Finally, in the Castro Marim wildfire, burning periods 3 and 4 overlapped in time. A progression polygon in the rear/right flank was delimited by fire personnel at 02:30, however the prior contiguous progression was identified at 16:30, suggesting a very low burning flank, opposite to the fast burning part of the wildfire southwards. This overlap had no effect on the average ROS, and only a very slight effect on the estimated FGR and FRE. However, users must be aware that burning periods seldom overlap (~4% registered in the entire dataset), which may have implications in subsequent analyses.

4 Discussion

4.1 The PT-FireSprd database

The PT-FireSprd is the first open access fire progression and behaviour database in the entire Mediterranean Europe. The progression of 80 large wildfires that occurred in mainland Portugal between 2015-2021 is reconstructed and fire behaviour descriptors such as ROS, FGR and FRE are estimated, dramatically expanding the extant information (Palheiro et al., 2006; Rodriguez y Silva & Molina-Martínez 2012; Fernandes et al., 2016). Wildfire progression was derived by converging evidence from multiple data sources, which provides added reliability to the database. Wide variability in fire behaviour is covered, tackling an important limitation pointed out by Cruz (2010). The approach presented will be used to update the database in the following years for Portugal, and can be replicated in other countries, depending on data availability.

The large number of fire behaviour observations, both at the polygon level (L2) and at the burning period level (L3), provide enough information for a wide variety of potential applications. Combined with detailed information on the drivers, namely weather and fuel, and effects, it can be used to: i) improve current knowledge on the drivers affecting the behaviour of large wildfires; ii) calibrate existing or new models which ultimately should help to better predict fire behaviour and support efficient fire management strategies (Alexander and Cruz, 2013a); iii) support the construction of case studies by fire analysts and contribute to better training of fire personnel (Alexander and Thomas, 2003); iv) contribute to improve operational fire suppression strategies; v) better understand how fire behaviour is linked to its effects (Collins et al., 2009), v) improve fire danger rating (Wotton, 2009); and vi) better characterize fire regimes (Pereira et al. 2022). In addition, the fire behaviour classes described in Figure 8 can assist fire suppression operations, including resources dispatching and decisions to fight or flee, or offensive vs defensive strategies.

For several reasons, it is easier to collect information for larger wildfires than for smaller ones. The wide range in fire sizes in the PT-FireSprd database suggests that it is representative of wildfires burning under a broad range of conditions. However, smaller wildfires (between 100 and 500 ha) are slightly under-represented in the database creating a potential bias. This can

be particularly relevant if one considers the high proportion of smaller wildfires that occur every year. Thus, fire behaviour descriptors may also be biased towards larger values that may have an implication, for example, on the calculated fire behaviour percentiles (Figure 8). Note that for typical fuel loads, say 15-20 t ha^{-1} (Fernandes et al., 2016), ROS between percentiles 50 and 75 already correspond to fires that are very difficult to control (Hirsch and Martell, 1996). The ROS and FRR historical distribution are a first approach with the aim of creating a simple and clear communication baseline between researchers and fire personnel based on quantitative fire behaviour data. Ultimately, the database will allow framing the behaviour of new wildfires according to historical patterns. Adding smaller wildfires to the PT-FireSprd database will certainly help to better represent a wider range of fire behaviour patterns.

Confidence in the wildfires of 2015-2016 was lower than for the most recent ones due to relevant advances in operational fire monitoring, resulting in better quality and higher quantity of fire data. Since 2018, the FEBMON system has improved and grown, providing larger quantity and higher quality data, thus leading to more reliable and detailed fire progression reconstructions. The distribution of the duration of the spread polygons between 2015 and 2021 (Figure B3) shows heterogeneity of the database across time, but also the evolution introduced along with FEBMON. Results suggest that ROS and FGR may be underestimated in wildfires with lower confidence, most probably due to the lack of data to thoroughly cover the afternoon, but especially the early night period (i.e. between VIIRS/MODIS day and nighttime overpasses, Figure 1). This issue is further discussed in section 5.2. The user must take into account the characteristics of the database and can choose to use the entire or part of the dataset based on the confidence flag or year of the wildfire.

The PT-FireSprd database is flexible and open, allowing the users to subset the data based on their needs and requirements. For example, users can decide to work with fire behaviour descriptors at the polygon level (L2) or at the burning period (L3), or can create their own subset depending on their objectives. The dataset is heterogeneous which is reflected in two main components: the duration of the spread polygons and the burning periods, and the confidence flag associated with each wildfire.

Regarding the duration, the average time elapsed between two progression polygons was 3h30 (L2) and 8h15 for the burning periods (L3). Durations were large in 2015 and 2016 (median values above 9h), decreased significantly in 2017 with the integration of hourly isochrones from Guerreiro et al., (2017, 2018), and had median durations below 2h since 2019 (Figure B3). Gollner et al., (2015) argued that fire progression observations need to be made in real-time with a 10 m spatial resolution every 10 min to meet the needs of fire behaviour forecasting. However, in operational context the current objective is to predict fire behaviour time intervals larger than or equal to 30 min (Cruz and Alexander, 2013). Considering the average duration of the burning periods, that represent a single fire run, the average time elapsed between progression observations represents a good compromise and a clear advance in current data. Regardless, users can subset the database based on the duration of either the progression polygons or the burning periods. L3 descriptors can be useful to provide more homogeneous and normalised

fire behaviour descriptors, dampening the effect of the large variability in L2 durations, allowing, for example, a better comparison between wildfires.

Finally, results suggest that considering both ROS and FGR can improve understanding of wildfire dynamics. The relation between both is dependent on perimeter morphology and extent (among others), and future work is needed to better understand the underlying factors. Most importantly, FGR was a better explanatory variable of burned area extent than ROS. The practical consequence is that large burned areas can be generated by wildfires with a moderate forward ROS but with large FGR, which in turn is highly influenced by spread duration and perimeter extent. This should have implications for both the research and operational communities. FRE was estimated for a lower number of spread polygons and burning periods when compared with ROS and FGR. This was most likely due to the impact of clouds and smoke on MSG-SEVIRI detections and the conservative minimum number of observations threshold (75 %). FRE and burned area extent were closely related, however, relations between FRE and ROS were poor/moderate. One of the possible reasons may be related with the need to consider the effect of the active perimeter extent when comparing both descriptors.

4.2 Limitations and future improvements

The generic limitations of the input data have been thoroughly described in Section 1. In particular, for Portugal some limitations of the data must be pointed out. Fire progression perimeters and fire points collected in the ground by fire personnel have relevant spatio-temporal uncertainties. For example, there is often a lag between the date/hour a polygon is drawn in the ground and the actual date/hour it burned completely. Another relevant issue is that of data acquisition / reporting errors done by fire personnel, which may be reduced by improved training and experience. The number of users of the FEBMON system has been growing in recent years and, with adequate training, it is expected that the quality and quantity of ground data will increase in upcoming years. In fact, over 27,000 aerial and 2,500 ground photos were taken in the year of 2022, which represents a relevant increase compared to previous years.

Regarding airborne data, the discussion may be separated into two components. First, initial attack photos, which can be extremely useful to draw initial fire progression and infer probable ignition areas, are not collected for every wildfire to which a helicopter is dispatched, and sometimes are of poor quality. Additional training and increasing the awareness of fire personnel for the relevance of the data they collect is necessary. Second, aircraft data are acquired at relatively low altitude, precluding a synoptic view of the wildfire. Time lags between data acquisition for different parts of the wildfire (e.g. left vs. right flanks) may be large and introduce relevant spatio-temporal uncertainties in the delineation of the fire progression. In addition, perimeters are drawn manually and depend on the training and experience of the fire expert. In upcoming years, the integration of new airborne sensors, specially with multispectral capability, the ability to perform high-altitude scans and the use of automatic perimeter delimitation procedures (e.g., Valero et al., 2018) should improve data quality and reduce the time lags of airborne fire observations. With this new capacity, it will be possible to integrate deep learning processes in the data analysis,

increasing both the quantity and quality of the available fire data. This integration will also allow a well-organised structure in data collection, management and analysis, improving decision-support systems. Finally, the use of UAVs during nighttime (pioneered in 2022 in Portugal) will complement aeroplane/helicopter data during periods of low data availability.

Regarding official fire data, errors in the delineation of burned area perimeters and in the ignition location, often located outside of the fire perimeter, need to be corrected to increase the quality of the PT-FireSprd database. Implementation of (semi-) automatic algorithms to delimit fire perimeters using satellite data (e.g., Chen et al., 2022) will increase data availability and reduce the uncertainties associated with manual perimeter delineation. Improvements in the spatial resolution geostationary satellites, such as the recently launched Meteosat Third Generation (MTG), will certainly improve fire behaviour estimates, as already observed in HIMAWARI-8 and last generation GOES satellites.

Concerning methodological uncertainties, the major challenge was to assign the correct date/hour to a specific burned area. For example, when raw data sources indicated that an area burned but active areas were absent or small, there were always uncertainties as to when it actually burned completely, which may lead to a relevant ROS/FGR underestimation. These uncertainties were larger between dusk until VIIRS overpass(es) and between the later and dawn. One approach to reduce these uncertainties was to use FRE data to monitor the daily cycle of fire activity and help to better define the start/end date of a progression polygon. The method was empirical and future work is needed to better define the thresholds for setting the ignition or reactivation times, as well as the end of a fire progression. Exploratory analysis done in a few wildfires of the PT-FireSprd database suggest that FRE has a significant drop after the head of the fire stops, which may take several minutes/hours until reaching the FRE thresholds used. This moment is commonly accompanied by flank growth that burns slower and releases lower amounts of energy. Such fire dynamics probably explain why ROS was likely underestimated in low confidence wildfires and why FGR was less affected by data confidence. Improvements can be achieved in the future, through the use of more sophisticated methods (e.g. change point detection), more ground observations during the head to flank run transition, and higher spatial resolution data from geostationary satellites. Part of these improvements can be used to partially update the 2015-2021 wildfires of the PT-FireSprd database.

In terms of characterising uncertainties and its effects, future work should also adopt a metrological approach to propagate uncertainties to the descriptors, providing useful information to users. By providing an uncertainty assessment, the PT-FireSprd database would be on the pathway to Fiducial Reference Measurement (FRM) compliance (Niro et al. 2021).

The continuous update of the PT-FireSprd database will require a joint effort by researchers and fire personnel. The automation of data collection procedures (discussed above), as well as dedicated training to fire personnel, are key factors to guarantee both the quality as well as a sustainable update of the database. In upcoming years, other fire behaviour descriptors may be included such as type of spread (surface vs. crown fire), fireline intensity, flame length, spotting (including maximum distance)

and/or PyroCb occurrence. Finally, methods described in the current work can be, at least partially, be applied to many other fire-prone areas of the globe and contribute to the much-needed data on observed wildfire behaviour.

5 Data Availability

The dataset contains generic metadata file with relevant information for each wildfire (Table A3), such as the fire ID, official incident ID (ANEPC, 13 digit number), fire name, municipality, civil parish, start date, duration (hours), extent (ha), among others. The fire name was defined as Municipality_DDMMYYYY, where DD is day, MM month and YYYY the year. In case that more than one wildfire occurred in the same municipality on the same day, we added an additional string at the end of the fire name (e.g. "_2").

The dataset is then divided in 3 Levels, in the corresponding folders:

- Fire Spread (L1): Each year has a separate folder that contains one folder per wildfire labelled with the fire name. It contains a polygon shapefile with the attributes listed in Table A4.
- Fire behaviour (L2): A single polygon shapefile that contains all wildfires and estimated fire behaviour metrics for each individual fire spread polygon. The attributes are listed and explained in Table A5.
- Fire behaviour (L3): A single polygons shapefile that contains the simplified fire behaviour metrics calculated for each burning period. The attributes are described in Table A6.

The generic metadata is connected to L1 data through the "fire name" field, and to L2 and L3 through the fire "ID" field.

The data are freely available at https://doi.org/10.5281/zenodo.7495506 (last access: 30th December 2022; Benali et al. 2022). We intend to update the database annually with wildfires from the current fire season and implement continuous improvements to the procedure. Also, if additional information from past wildfires becomes available, we will update the database either by changing existing fire spread polygons or by adding new wildfires. Updates for future years depend on the availability of input data and associated funding.

6 Conclusions

The Portuguese Large Wildfire Spread Database (PT-FireSprd) is the first open access fire progression and behaviour database available within Mediterranean Europe. It includes the reconstruction of the progression of 80 large wildfires (>100 ha) that occurred in mainland Portugal between 2015 and 2021, which was derived by seeking converging evidence from multiple data sources. PT-FireSprd contains a very large number estimates of key fire behaviour descriptors, such as ROS, FGR and FRE. Based on the statistical distribution of ROS and FGR, we defined 6 percentile intervals that can be easily communicated to

both research and management communities and to support a wide number of applications, including better fire management strategies. The PT-FireSprd has a large potential to contribute to the development of better fire behaviour prediction tools, improve our current knowledge on wildfire dynamics, foster better operational training and contribute to improve decision-making. The approach will be used to continuously update the database in the following years for Portugal and can be replicated in other countries/regions, depending on data availability. Improvements in data quality and the implementation of automated methods are key factors for the regular update of the PT-FireSprd database in the future.

Appendix A: Supporting material for the Methods

(Table A1, Table A2, Table A3, Table A4, Table A5 and Table A6 near here)

Appendix B: Supporting material for the Results

(Figure B1, Figure B2 and Figure B3 near here)

Author Contribution

AB and FS designed the study. AB, NG, HG, CM, JS carried out data processing and delimited fire progressions. BM carried out FRE data processing. AB assembled the database, performed data analysis and wrote the first version of the manuscript. All authors contributed to the interpretation of the results and writing of the manuscript.

Competing interests

The authors declare that they have no conflict of interest.

Acknowledgements

We thank Florian Briquemont for initial data processing and progression delimitation; FEPC personnel provided relevant fire to reconstruct some of the wildfires: Pedro Machado, Eduardo Marques, Marco Pires, Marco Lucas, Miguel Martins, Daniel Santana and Vítor Caramelo. We would also like to thank other fire personnel who provided relevant fire data: João Pedro Costa (AFOCELCA), José Silva (AFOCELCA), António Louro (CM-Mação), Sónia Oliveira (CM-Mação), Rui Lopes (CBV Peso da Régua), Amélia Freitas (CM Caminha), Rui Pedro Fernandes (CBV Valença), Carlos Gomes (CBV Boticas), António Ribeiro (ANEPC), Mário Silvestre (ANEPC), Emanuel Oliveira, and Elisio Pereira (CBV Porto de Mós). Finally, we would like to thank ANEPC and FEPC for providing full access to their fire data enabling the development of the entire work.

This research was supported by the Forest Research Centre, a research unit funded by Fundação para a Ciência e a Tecnologia I.P. (FCT), Portugal (UIDB/00239/2020), project foRester (PCIF/SSI/0102/2017) and FIRE-MODSAT II (PTDC/ASP-SIL/28771/2017) also funded by FCT.

Akli Benali was funded by FCT through a CEEC contract (CEECIND/03799/2018/CP1563/CT0003). Nuno Guiomar was funded by the European Union through the European Regional Development Fund in the framework of the Interreg V-A Spain-Portugal program (POCTEP) under the CILIFO (Ref. 0753_CILIFO_5_E) and FIREPOCTEP (Ref. 0756_FIREPOCTEP_6_E) projects and by National Funds through FCT under the Project UIDB/05183/2020. Paulo Fernandes contributed in the framework of the FCT-funded project UIDB/04033/2020. Ana Sá was supported under the framework of the contract-program nr. 1382 (DL 57/2016/CP1382/CT0003).

References

Albini, F. A.: Wildland Fires: Predicting the behavior of wildland fires—among nature's most potent forces—can save lives, money, and natural resources, Am. Sci., 72(6), 590-597, 1984.

Alcasena, F., Ager, A., Le Page, Y., Bessa, P., Loureiro, C., and Oliveira, T.: Assessing wildfire exposure to communities and protected areas in Portugal, Fire, 4(4), 82, doi:10.3390/ fire404008, 2021.

Alexander, M., and Cruz, M. G.: Are the applications of wildland fire behaviour models getting ahead of their evaluation again?, Environ. Model. Softw. (41), 65-71, doi:10.1016/j.envsoft.2012.11.001, 2013.

Alexander M. E., and Cruz M. G.: Evaluating a model for predicting active crown fire rate of spread using wildfire observations, Can. J. For. Res.,36, 3015–3028, doi:10.1139/x06-174, 2006.

Alexander, M. E., and Lanoville, R. A.: Wildfires as a source of fire behavior data: a case study from Northwest Territories, Canada. 9th Conf. Fire and Forest Meteorology, April 21-24, San Diego, CA. American Meteorological Society, Boston, Mass, 86-93, 1987.

Alexander, M. E., and Thomas, D. A.: Wildland fire behavior case studies and analyses: Other examples, methods, reporting standards, and some practical advice, Fire Manag. Today, 63(4), 4-12, 2003

Andela, N., Morton, D. C., Giglio, L., Paugam, R., Chen, Y., Hantson, S., van der Werf, G. R., and Randerson, J. T.: The Global Fire Atlas of individual fire size, duration, speed and direction, Earth Syst. Sci. Data, 11(2), 529-552, doi:10.5194/essd-11-529-2019, 2019.

Anderson, W. R., Cruz, M. G., Fernandes, P. M., McCaw, L., Vega, J. A., Bradstock, R. A., Fogarty, L .G., Gould, J. B., McCarthy, G. H., Marsden-Smedley, J. B., Matthews, S., Mattingley, G., Pearce, H .G., and van Wilgen, B. W.: A generic, empirical-based model for predicting rate of fire spread in shrublands, Int. J. Wildland Fire, 24(4), 443-460, doi:10.1071/WF14130, 2015.

Artés, T., Oom, D., De Rigo, D., Durrant, T. H., Maianti, P., Libertà, G., and San-Miguel-Ayanz, J.: A global wildfire dataset for the analysis of fire regimes and fire behaviour, Sci. Data, 6(1), 1-11, doi:10.1038/s41597-019-0312-2, 2019.

Benali, A., Guiomar, N., Gonçalves, H., Mota, B., Silva, F., Fernandes, P.M., Mota, C., Penha, A., Santos, J., Pereira, J.M.C., and Sá, A.C.L: The Portuguese Large Wildfire Spread Database (PT-FireSprd), https://doi.org/10.5281/zenodo.7495506 , 2022.

Briones-Herrera, C. I., Vega-Nieva, D. J., Monjarás-Vega, N. A., Briseño-Reyes, J., López-Serrano, P .M., Corral-Rivas, J. J., Alvarado-Celestino, E., Arellano-Pérez, S., Álvarez-González, J.G., Ruiz-González, A. D., Jolly, W. M., and Parks, S. A.: Near real-time automated early mapping of the perimeter of large forest fires from the aggregation of VIIRS and MODIS active fires in Mexico, Remote Sens., 12(12), 2061, doi:10.3390/rs12122061, 2020.

Butler, B. W., and Reynolds, T. D.: Wildfire case study: Butte City, southeastern Utah, July 1, 1994, USDA For. Serv., Intermt. Res. Stn., Ogden, UT. Gen. Tech. Rep. INT-GTR-351, doi:10.2737/INT-GTR-351, 1997.

Catchpole, W. R., Catchpole, E. A., Butler, B. W., Rothermel, R. C., Morris, G. A., and Latham, D. J.: Rate of spread of free-burning fires in woody fuels in a wind tunnel, Combust. Sci. Technol., 131(1-6), 1-37, doi:10.1080/00102209808935753, 1998.

Chen, Y., Hantson, S., Andela, N., Coffield, S. R., Graff, C. A., Morton, D. C., Ott, L.E., Foufoula-Georgiou, E., Smyth, P., Goulden, M .L., and Randerson, J. T.: California wildfire spread derived using VIIRS satellite observations and an object-based tracking system, Sci. Data, 9(1), 1-15, doi:10.1038/s41597-022-01343-0, 2022.

Cheney, N. P., Gould, J. S., McCaw, W .L., and Anderson, W. R.: Predicting fire behaviour in dry eucalypt forest in southern Australia,. For. Ecol. Manag., 280, 120-131, doi:10.1016/j.foreco.2012.06.012, 2012.

Cheney, N. P.: Fire behaviour during the Pickering Brook wildfire, January 2005 (Perth Hills Fires 71-80), Conserv. Sci. West. Aust., 7, 451–468, 2010.

Cheney, N., Gould, J., and Catchpole, W.: The Influence of Fuel, Weather and Fire Shape Variables on Fire-Spread in Grasslands, Int. J. Wildland Fire, 3, 31, doi:10.1071/WF9930031, 1993.

Coen, J. L., and Riggan, P. J.: Simulation and thermal imaging of the 2006 Esperanza Wildfire in southern California: application of a coupled weather–wildland fire model, Int. J. Wildland Fire, 23(6), 755-770, doi:10.1071/WF12194, 2014.

Collins, B. M., Miller. J. D., Thode, A. E., Kelly, M., van Wagtendonk, J. W., and Stephens, S. L.: Interactions among wildland fires in a long- established Sierra Nevada natural fire area, Ecosystems 12, 114–128, doi:10.1007/s10021-008-9211-7, 2019.

Countryman, C. M.: The fire environment concept, USDA Forest Service, Pacific Southwest Range and Experiment Station, Berkeley, California, USA, 1972.

Crowley, M. A., Cardille, J. A., White, J. C., and Wulder, M. A.: Generating intra-year metrics of wildfire progression using multiple open-access satellite data streams, Remote Sens. Environ., 232, 111295, doi:10.1016/j.rse.2019.111295, 2019.

Cruz, M. G., Alexander, M. E., and Kilinc, M.: Wildfire rates of spread in grasslands under critical burning conditions, Fire, 5(2), 55, doi:10.3390/fire5020055, 2022.

Cruz, M. G., Cheney, N. P., Gould, J. S., McCaw, W. L., Kilinc, M., and Sullivan, A. L.: An empirical-based model for predicting the forward spread rate of wildfires in eucalypt forests, Int. J. Wildland Fire, 31(1), 81-95, doi:10.1071/WF21068, 2021.

Cruz, M. G., and Alexander, M. E.: The 10% wind speed rule of thumb for estimating a wildfire's forward rate of spread in forests and shrublands, Ann. For. Sci., 76(2), 1-11, doi:10.1007/s13595-019-0829-8,2019.

Cruz, M. G., Alexander, M. E., Sullivan, A. L., Gould, J. S., and Kilinc, M.: Assessing improvements in models used to operationally predict wildland fire rate of spread, Environ. Model. Softw., 105, 54-63, doi:10.1016/j.envsoft.2018.03.027, 2018.

Cruz, M. G., Gould, J. S., Alexander, M. E., Sullivan, A. L., McCaw, W. L., and Matthews, S.: Empirical-based models for predicting head-fire rate of spread in Australian fuel types, Aust. For., 78(3), 118-158, doi:10.1080/00049158.2015.1055063, 2015.

Cruz, M. G., McCaw, W. L., Anderson, W. R., and Gould, J. S.: Fire behaviour modelling in semi-arid mallee-heath shrublands of southern Australia, Environ. Model. Softw., 40, 21-34, doi:10.1016/j.envsoft.2012.07.003, 2013.

Cruz, M. G., and Alexander, M. E.: Uncertainty associated with model predictions of surface and crown fire rates of spread, Environ. Model. Softw., 47, 16-28, doi:10.1016/j.envsoft.2013.04.004, 2013.

Cruz, M. G.: Monte Carlo-based ensemble method for prediction of grassland fire spread, Int. J. Wildland Fire, 19(4), 521-530, doi:10.1071/WF08195, 2010.

Cruz, M. G., Alexander, M.E., and Wakimoto, R.H.: Development and testing of models for predicting crown fire rate of spread in conifer forest stands, Can. J. For. Res., 35(7), 1626-1639, doi:10.1139/x05-085, 2005.

Dale, M. R. T., and Fortin, M. J.: From graphs to spatial graphs, Annu. Rev. Ecol. Evol. Systs., 21-38, doi:10.1146/annurev-ecolsys-102209-144718, 2010.

Duff, T. J., Chong, D. M., and Tolhurst, K. G.: Quantifying spatio-temporal differences between fire shapes: Estimating fire travel paths for the improvement of dynamic spread models, Environ. Model. Softw, 46, 33-43, doi:10.1016/j.envsoft.2013.02.005, 2013.

Fernandes, P. M., Sil, A., Ascoli, D., Cruz, M. G., Rossa, C. G., and Alexander, M. E.: Characterizing fire behavior across the globe. In: Hood, S. M., Drury, S., Steelman, T., Steffens, R.[eds.]: Proceedings of the Fire Continuum-Preparing for the future of wildland fire; 2018 May 21-24; Missoula, MT. Proceedings RMRS-P-78. Fort Collins, CO: US Department of Agriculture, Forest Service, Rocky Mountain Research Station. p. 258-263., 78, 258-263, 2020.

Fernandes, P. M., Sil, A., Ascoli, D., Cruz, M. G., Alexander, M. E., Rossa, C. G., Baeza, J., Burrows, N., Davies, G. M., Fidelis, A., Gould, J. S., Govender, N., Kilinc, M., and McCaw, L.: Drivers of wildland fire behaviour variation across the Earth. In: Viegas, D.X. (Ed.), Advances in Forest Fire Research, Chapter 7 – Short contributions, 1267-1270, doi:10.14195/978-989-26-16-506_154, 2018.

Fernandes, P. M., Barros, A. M., Pinto, A., and Santos, J. A.: Characteristics and controls of extremely large wildfires in the western Mediterranean Basin, J. Geophys. Res. Biogeosci., 121(8), 2141-2157, doi:10.1002/2016JG003389, 2016.

Fernandes, P. M., Botelho, H.S., Rego, F.C., and Loureiro, C.: Empirical modelling of surface fire behaviour in maritime pine stands, Int. J. Wildland Fire, 18(6), 698-710, doi:10.1071/WF08023, 2009.

Finney, M. A., McAllister, S. S., Forthofer, J. M., and Grumstrup, T. P.: Wildland Fire Behaviour: Dynamics, Principles and Processes, CSIRO Pub., 2021.

Forestry Canada Fire Danger Group: Development and structure of the Canadian Forest Fire Behavior Prediction System. For. Can., Ottawa, Ont. Inf. Rep. ST-X-3, 1992.

Frantz, D., Stellmes, M., Röder, A., and Hill, J.: Fire spread from MODIS burned area data: Obtaining fire dynamics information for every single fire, Int. J. Wildland Fire, 25(12), 1228-1237, doi:10.1071/WF16003, 2016.

Giglio, L., Descloitres, J., Justice, C. O., and Kaufman, Y. J.: An enhanced contextual fire de- tection algorithm for MODIS, Remote Sens. Environ. 87, 273–282, doi:10.1016/S0034-4257(03)00184-6, 2003

Giglio, L., Schroeder, W. and Justice, C. O.: The collection 6 MODIS active fire detection algorithm and fire products. Remote Sens. Environ., 178, pp.31-41, doi:10.1016/j.rse.2016.02.054, 2016.

Gollner, M., Trouve, A., Altintas, I., Block, J., de Callafon, R., Clements, C., Cortes, A., Ellicott, E., Filippi, J. B., Finney, M., Ide, K., Jenkins, M.A., Jimenez, D., Lautenberger, C., Mandel, J., Rochoux, M., and Simeoni, A.: Towards data-driven operational wildfire spread modeling: A report of the NSF-funded WIFIRE workshop, 2015.

Guerreiro, J., Fonseca, C., Salgueiro, A., Fernandes, P., Iglésias, E. L., Neufville, R., Mateus, P., Castellnou, M., Silva, J. S., Moura, J. M., Rego, F. C., and Caldeira, D.: Análise e apuramento dos factos relativos aos incêndios que ocorreram em Pedrogão Grande, Castanheira de Pêra, Ansião, Alvaiázere, Figueiró dos Vinhos, Arganil, Góis, Penela, Pampilhosa da Serra, Oleiros e Sertã, entre 17 e 24 de junho de 2017. Comissão Técnica Independente, Assembleia da República, Lisboa. https://www.parlamento.pt/Documents/2017/Outubro/RelatórioCTI_VF.pdf, 2017.

Guerreiro, J., Fonseca, C., Salgueiro, A., Fernandes, P., Iglésias, E. L., Neufville, R., Mateus, P., Castellnou, M., Silva, J. S., Moura, J. M., Rego, F. C., and Caldeira, D.: Avaliação dos Incêndios ocorridos entre 14 e 16 de outubro de 2017 em Portugal Continental. Comissão Técnica Independente, Assembleia da República, Lisboa. https://www.parlamento.pt/Documents/2018/Marco/RelatorioCTI190318N.pdf, 2018.

Humber, M., Zubkova, M., and Giglio, L.: A remote sensing-based approach to estimating the fire spread rate parameter for individual burn patch extraction, Int. J. Remote Sens., 43(2), 649-673, doi:10.1080/01431161.2022.2027544, 2022.

Hirsch, K. G., and Martell, D. L. A review of initial attack fire crew productivity and effectiveness, Int. J. Wildland Fire, 6(4), 199-215, doi:10.1071/WF9960199, 1996.

Khanmohammadi, S., Arashpour, M., Golafshani, E. M., Cruz, M. G., Rajabifard, A., and Bai, Y.: Prediction of wildfire rate of spread in grasslands using machine learning methods, Environ. Model. Softw., 156, 105507, doi:10.1016/j.envsoft.2022.105507, 2022.

Kilinc, M., Anderson, W., and Price, B.: The Applicability of Bushfire Behaviour Models in Australia. Victorian Government, Department of Sustainability and Environment. DSE Schedule 5: Fire Severity Rating Project, Melbourne, VIC. Technical Report 1, 2012.

McCaw, W. L., Gould, J. S., Cheney, N. P., Ellis, P. F. M., and Anderson, W. R.: Changes in behaviour of fire in dry eucalypt forest as fuel increases with age, For. Ecol. Manag. 271, 170-181, doi:10.1016/j.foreco.2012.02.003, 2012.

Niro, F., Goryl, P., Dransfeld, S., Boccia, V., Gascon, F., Adams, J., Themann, B., Scifoni, S. and Doxani, G.: European Space Agency (ESA) Calibration/Validation Strategy for Optical Land-Imaging Satellites and Pathway towards Interoperability, Remote Sens., 13, 3003, doi:10.3390/rs13153003, 2021.

Oom, D., Silva, P. C., Bistinas, I., and Pereira, J. M. C.: Highlighting biome-specific sensitivity of fire size distributions to time-gap parameter using a new algorithm for fire event individuation, Remote Sens., 8(8), 663, doi:10.3390/rs8080663, 2016.

Palaiologou, P., Kalabokidis, K., Ager, A. A., and Day, M. A.: Development of Comprehensive Fuel Management Strategies for Reducing Wildfire Risk in Greece, Forests, 11(8), 789, doi:10.3390/f11080789, 2020.

Palheiro, P. M., Fernandes, P. M., Cruz, M. G.: A fire behaviour-based fire danger classification for maritime pine stands: comparison of two approaches, For. Ecol. Manag., (234), S54, doi:10.1016/j.foreco.2006.08.075, 2006.

Parisien M. A., Parks S. A., Miller C., Krawchuk M. A., Heathcott M., and Moritz M. A.: Contributions of ignitions, fuels, and weather to the burn probability of a boreal landscape, Ecosystems 14, 1141–1155, doi:10.1007/s10021-011-9474-2, 2011.

Parks, S. A.: Mapping day-of-burning with coarse-resolution satellite fire-detection data, Int. J. Wildland Fire, 23(2), 215-223, doi:10.1071/WF13138, 2014.

Pereira, M. G., Malamud, B. D., Trigo, R. M., and Alves, P.I.: The history and characteristics of the 1980–2005 Portuguese rural fire database, Nat. Hazards Earth Syst. Sci., 11(12), 3343-3358, doi:10.5194/nhess-11-3343-2011, 2011.

Pereira, J. M., Oom, D., Silva, P. C., and Benali, A.: Wild, tamed, and domesticated: Three fire macroregimes for global pyrogeography in the Anthropocene, Ecol. Appl., 32(6), e2588, doi:10.1002/eap.2588, 2022.

Pinto, M. M., DaCamara, C. C., Trigo, I. F., Trigo, R. M., and Turkman, K. F.: Fire danger rating over Mediterranean Europe based on fire radiative power derived from Meteosat, Nat. Hazards Earth Syst. Sci., 18(2), 515-529, doi:10.5194/nhess-2017-346, 2018.

Rodríguez y Silva, F., and Molina-Martínez, J.R.: Modeling Mediterranean forest fuels by integrating field data and mapping tools, Eur. J. For. Res., 131, 571–582, doi:10.1007/s10342-011-0532-2, 2012.

Rothermel, R.C.: A mathematical model for predicting fire spread in wildland fuels, Res. Pap. INT-115. Ogden, UT: U.S. Department of Agriculture, Intermountain Forest and Range Experiment Station, 1972.Sá, A. C., Benali, A., Fernandes, P. M., Pinto, R. M., Trigo, R. M., Salis, M., Russo, A., Jerez, S., Soares, P. M. M., Schroeder, W., and Pereira, J. M. C.: Evaluating fire growth simulations using satellite active fire data, Remote Sens. Environ., 190, 302-317, doi:10.1016/j.rse.2016.12.023, 2017.

Salis, M., Del Giudice, L., Arca, B., Ager, A. A., Alcasena-Urdiroz, F., Lozano, O., Bacciu, V., Spano, D., and Duce, P.: Modeling the effects of different fuel treatment mosaics on wildfire spread and behavior in a Mediterranean agro-pastoral area. J. Environ. Manage., 212, 490-505, doi:10.1016/j.jenvman.2018.02.020, 2018.

Santoni, P.-A., J.-B. Filippi, J.-H. Balbi, and Bosseur, F.: Wildland fire behaviour case studies and fuel models for landscape-scale fire modeling, J. Combust., 613424, doi:10.1155/2011/613424, 2011.

Schag, G. M., Stow, D. A., Riggan, P. J., Tissell, R. G., and Coen, J. L.: Examining landscape-scale fuel and terrain controls of wildfire spread rates using repetitive airborne thermal infrared (ATIR) imagery, Fire, 4(1), 6, doi:10.3390/fire4010006, 2021.

Schroeder, W., Oliva, P., Giglio, L., and Csiszar, I. A.: The New VIIRS 375 m active fire detection data product: Algorithm description and initial assessment, Remote Sens. Environ., 143, 85-96, doi:10.1016/j.rse.2013.12.008, 2014.

Schroeder, W.: Visible Infrared Imaging Radiometer Suite (VIIRS) 375 m & 750 m Active Fire Detection Data Sets Based on NASA VIIRS Land Science Investigator Processing System (SIPS) Reprocessed Data—Version 1. 2017.

Scott, J. H., and Reinhardt, E. D.: Assessing Crown Fire Potential by Linking Models of Surface and Crown Fire Behavior, US Department of Agriculture, Forest Service, Rocky Mountain Research Station, Fort Collins, CO. Research Paper RMRS-RP-29, doi:10.2737/RMRS-RP-29, 2001.

Sharples, J. J., McRae, R. H., and Wilkes, S. R.: Wind–terrain effects on the propagation of wildfires in rugged terrain: fire channelling, Int. J. Wildland Fire, 21(3), 282-296, doi:10.1071/WF10055, 2012.

Sifakis, N. I., Iossifidis, C., Kontoes, C., and Keramitsoglou, I.: Wildfire detection and tracking over Greece using MSG-SEVIRI satellite data, Remote Sens., 3(3), 524-538, doi:10.3390/rs3030524, 2011.

Stocks, B. J., Alexander, M. E., Wotton, B. M., Stefner, C. N., Flannigan, M. D., Taylor, S. W., Lavoie, N., Mason, J. A., Hartley, G. R., Maffey, M. E., Dalrymple, G. N., Blake, T. W., and Cruz, M. G., Lanoville, R. A.: Crown fire behaviour in a northern jack pine black spruce forest, Can. J. For. Res. 34, 1548-1560, doi:10.1139/x04-054, 2004.

Storey, M. A., Price, O. F., Sharples, J. J., and Bradstock, R. A.: Drivers of long-distance spotting during wildfires in south-eastern Australia, Int. J. Wildland Fire, 29(6), 459-472, doi:10.1071/WF19124, 2020.

Storey, M. A., Bedward, M., Price, O. F., Bradstock, R. A., and Sharples, J. J.: Derivation of a Bayesian fire spread model using large-scale wildfire observations, Environ. Model. Softw., 144, 105127, doi:10.1016/j.envsoft.2021.105127, 2021.

Stow, D.A., Riggan, P.J., Storey, E.A., and Coulter, L.L.: Measuring fire spread rates from repeat pass airborne thermal infrared imagery. Remote Sens. Lett., 5, 803–812, doi:10.1080/2150704X.2014.967882, 2014.

Vaillant, N. M., Ewell, C.M., and Fites-Kaufman, J. A.: Capturing crown fire behavior on wildland fires - the Fire Behavior Assessment Team in action, Fire Manag. Today 73(4):41-45, 2014.

Valero, M. M., Rios, O., Pastor, E., and Planas, E.: Automated location of active fire perimeters in aerial infrared imaging using unsupervised edge detectors, Int. J. Wildland Fire, 27(4), 241-256, doi:10.1071/WF17093, 2018.

Veraverbeke, S., Sedano, F., Hook, S. J., Randerson, J. T., Jin, Y., and Rogers, B. M.: Mapping the daily progression of large wildland fires using MODIS active fire data, Int. J. Wildland Fire, 23(5), 655-667, doi:10.1071/WF13015, 2014.

Viegas, D. X., Almeida, M. F., Ribeiro, L. M., Raposo, J., Viegas, M. T., Oliveira, R., Alves, D., Pinto, C., Rodrigues, A., Ribeiro, C., Lopes, S., Jorge, H., and Viegas, C. X.: Análise dos Incêndios Florestais Ocorridos a 15 de outubro de 2017, Centro de Estudos sobre Incêndios Florestais (CEIF/ADAI/LAETA), 2019.

Wade, D. D., and Ward, D. E.: An analysis of the Air Force Bomb Range Fire. Res. Pap. SE–105. Asheville, NC, USDA Forest Service, Southeastern Forest Experiment Station, 1973.

Wolfe, R. E., Roy, D. P., and Vermote, E.: MODIS land data storage, gridding, and compositing methodology: level 2 grid, IEEE Trans. Geosci. Remote Sens. 36, doi:10.1109/36.701082, 1998.

Wooster, M. J., Roberts, G., Freeborn, P. H., Xu, W., Govaerts, Y., Beeby, R., He, J., Lattanzio, A., Fisher, D., and Mullen, R.: LSA SAF Meteosat FRP products – Part 1: Algorithms, product contents, and analysis, Atmos. Chem. Phys., 15, 13217–13239, doi:10.5194/acp-15-13217-2015, 2015.

Wotton, B. M.: Interpreting and using outputs from the Canadian Forest Fire Danger Rating System in research applications, Environ. Ecol. Stat., 16(2), 107-131, doi:10.1007/s10651-007-0084-2, 2009.

928 **Figures**

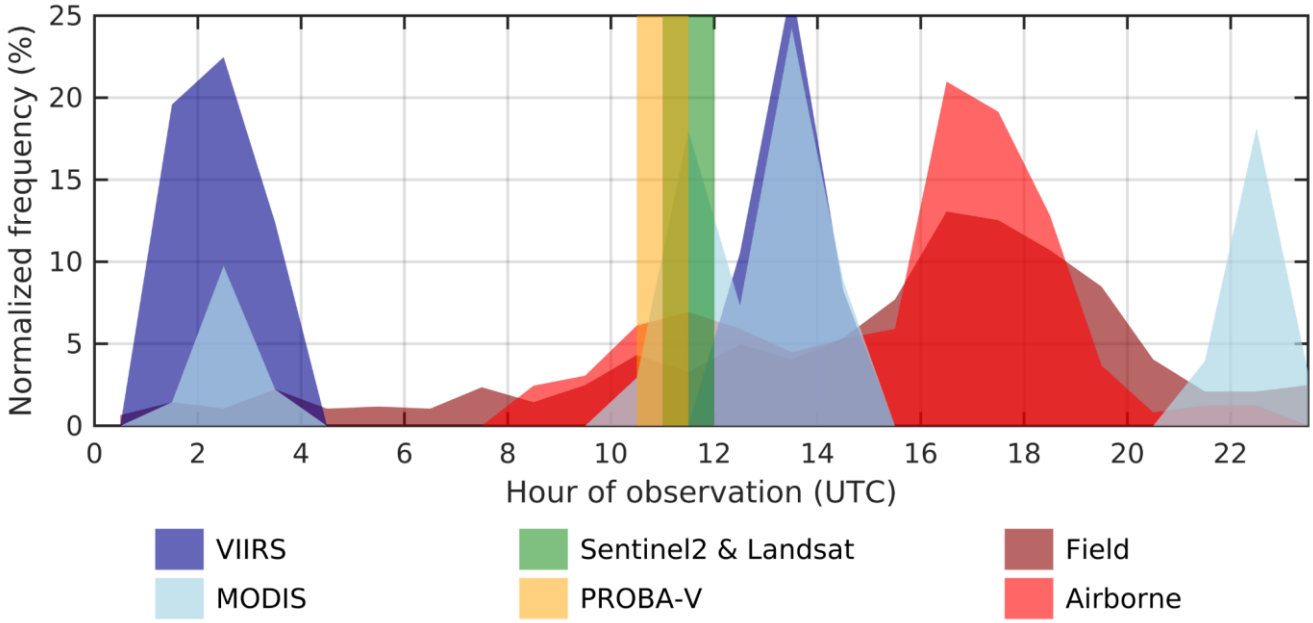

929

930

931 **Figure 1: Hourly frequency of observations in active wildfires acquisitions for satellite, field and airborne data. The data used refers**
932 **to the year 2019 as an example. The frequency is normalised by dividing the number of observations by the total of each data source.**
933 **Sentinel-2, Landsat and PROBA-V refer to the temporal windows and not the frequency, since all of the data are acquired in a very**
934 **short window. The time windows of Sentinel-3 are similar to those of MODIS. MSG-SEVIRI data are not represented since it has a**
935 **15' frequency. Acronyms are described in the Data and Methods section.**

936

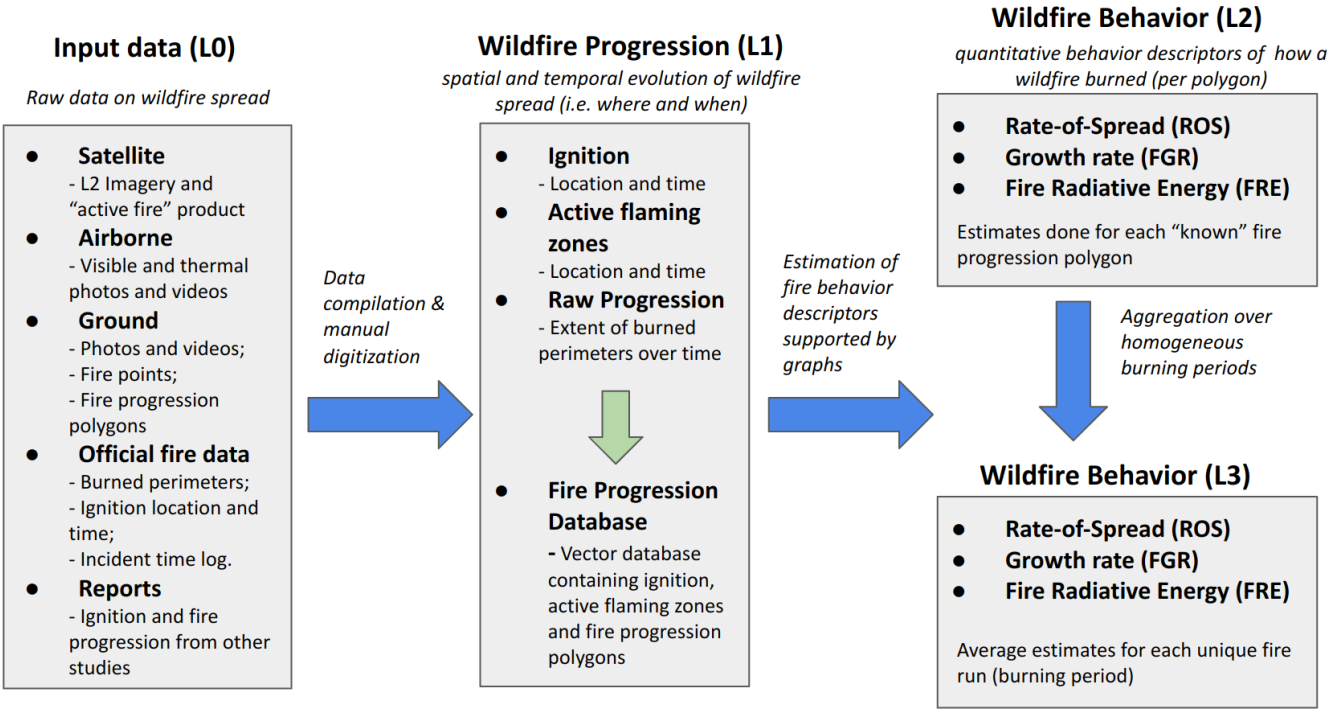

Figure 2: Flowchart that represents an overview of the data and methods used in the development of the PT-FireSprd database.

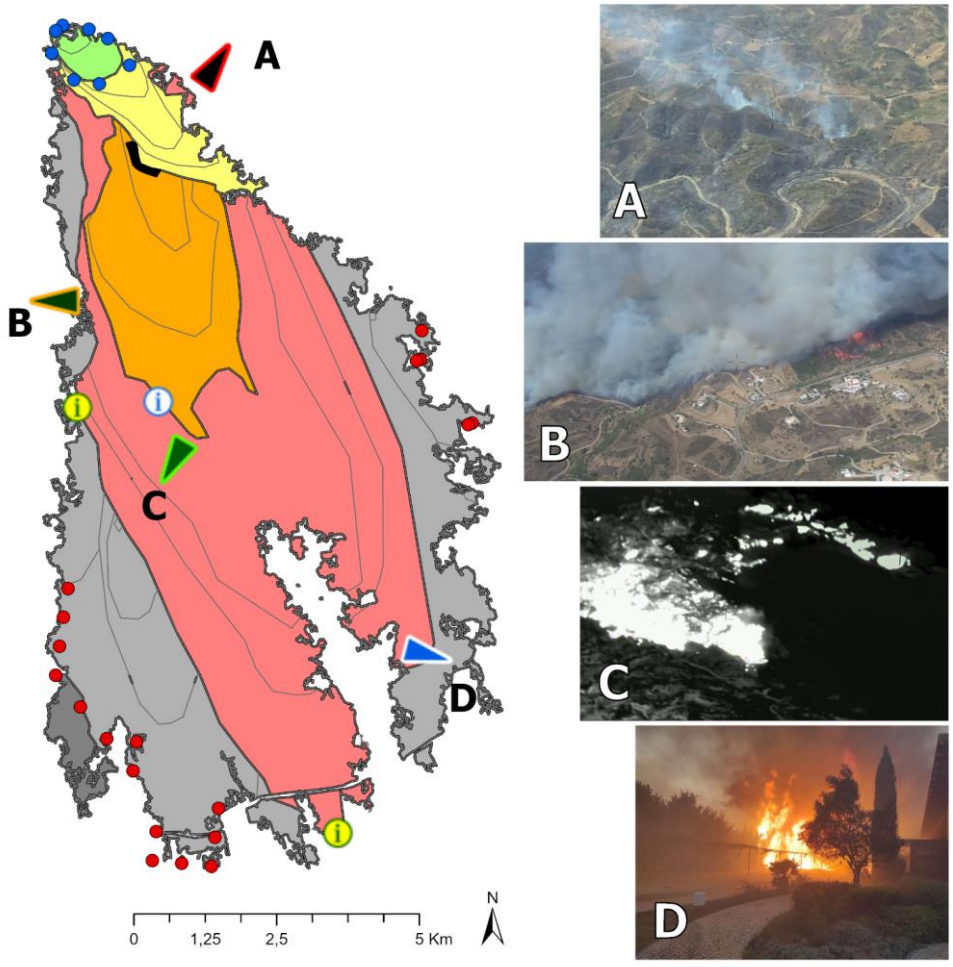

Figure 3: Example of multi-source data integration to derive fire perimeters and reconstruct the progression of the Castro Marim (2021) wildfire. The lines represent different progression polygons. Photos A, B, C, D were kindly provided by ANEPC\FEPC

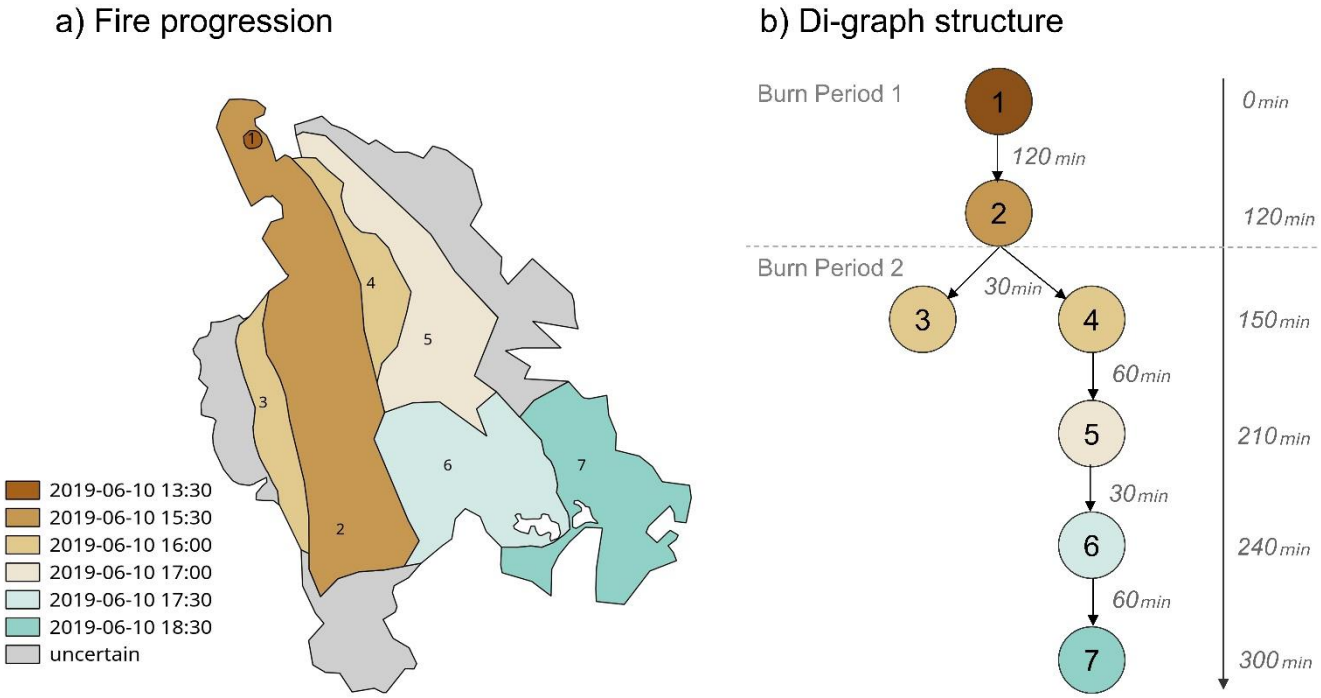

946
947

948 **Figure 4: Example of how the estimated fire progression of the Ourique 2019 wildfire (a) was used to build the digraph (b). Each**
949 **node corresponds to a fire progression polygon, identified in (a), and the edges correspond to the time elapsed (in minutes) between**
950 **each node.**

951

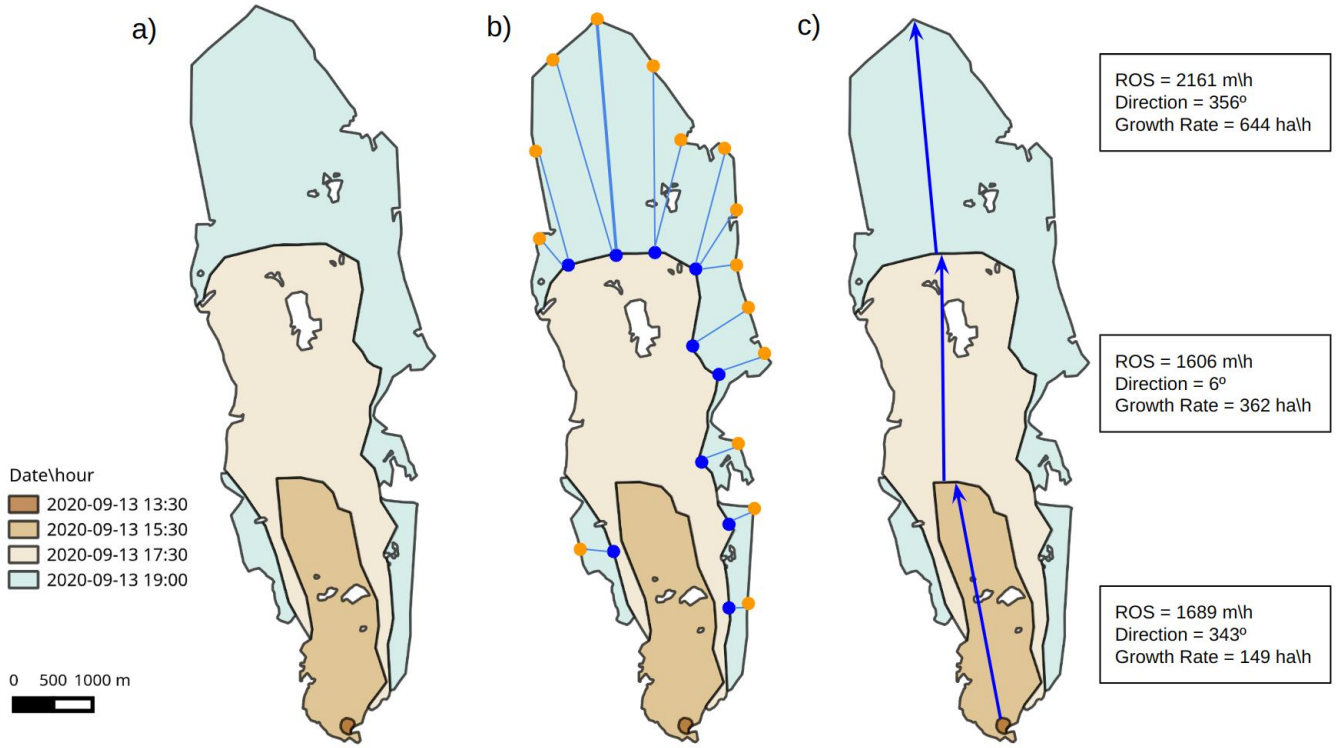

952

953

954 **Figure 5: Example of how the fire behaviour descriptors are calculated based on the Proença-a-Nova (2020) wildfire: a) partial fire**
955 **progression; b) procedure to calculate the distance for each vertex of the pair of consecutive polygons; and c) estimated main spread**
956 **axis and associated fire behaviour descriptors.**

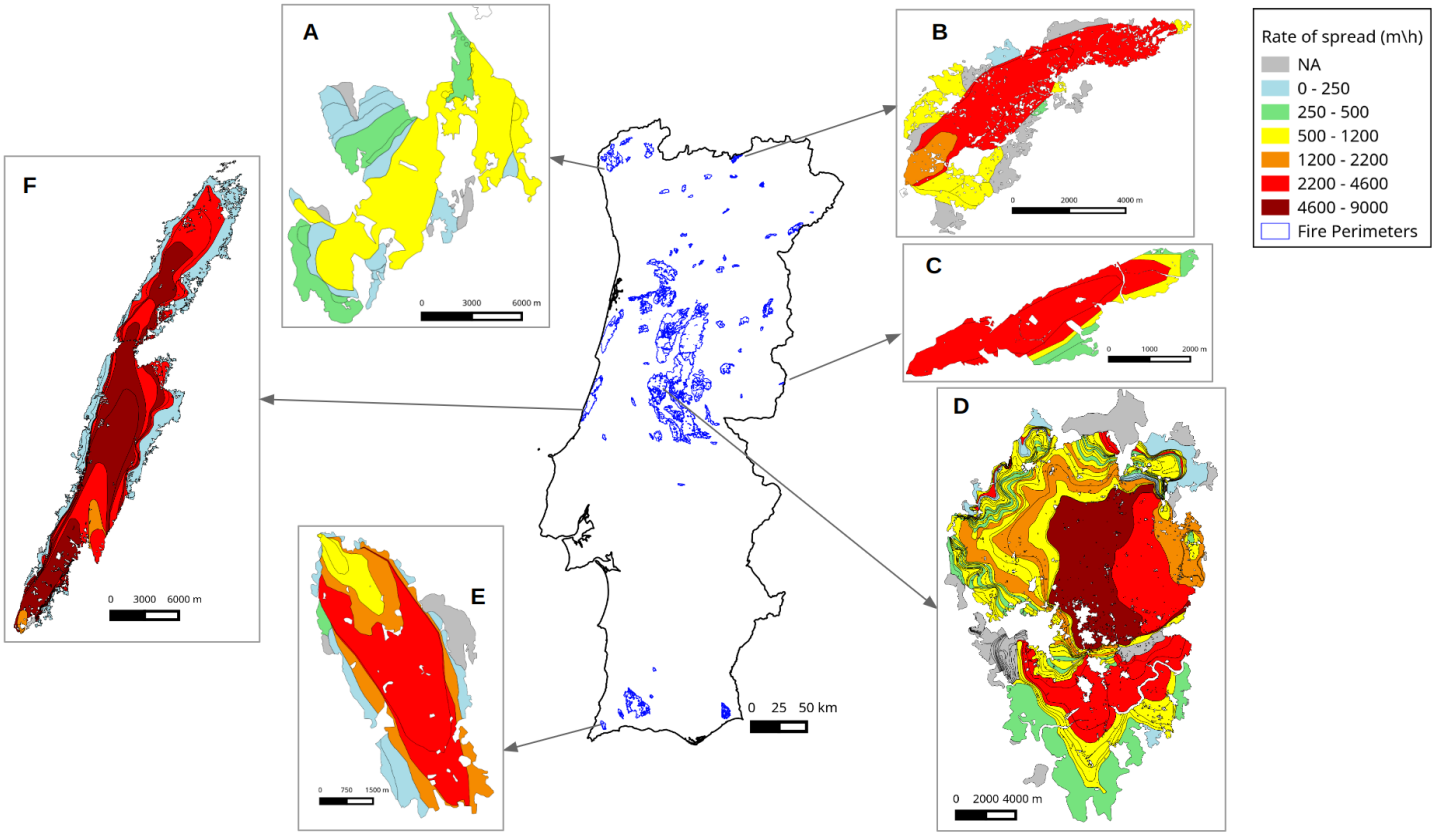

Figure 6: Overall spatial distribution of the wildfire perimeters in the PT-FireSprd database, with examples of ROS estimates for 6 wildfires: A-Paredes de Coura (2016); B-Chaves (2020); C-Idanha-a-Nova (2020); D-Pedrógão Grande (2017); E-Aljezur (2020); F-Alcobaça (2017).

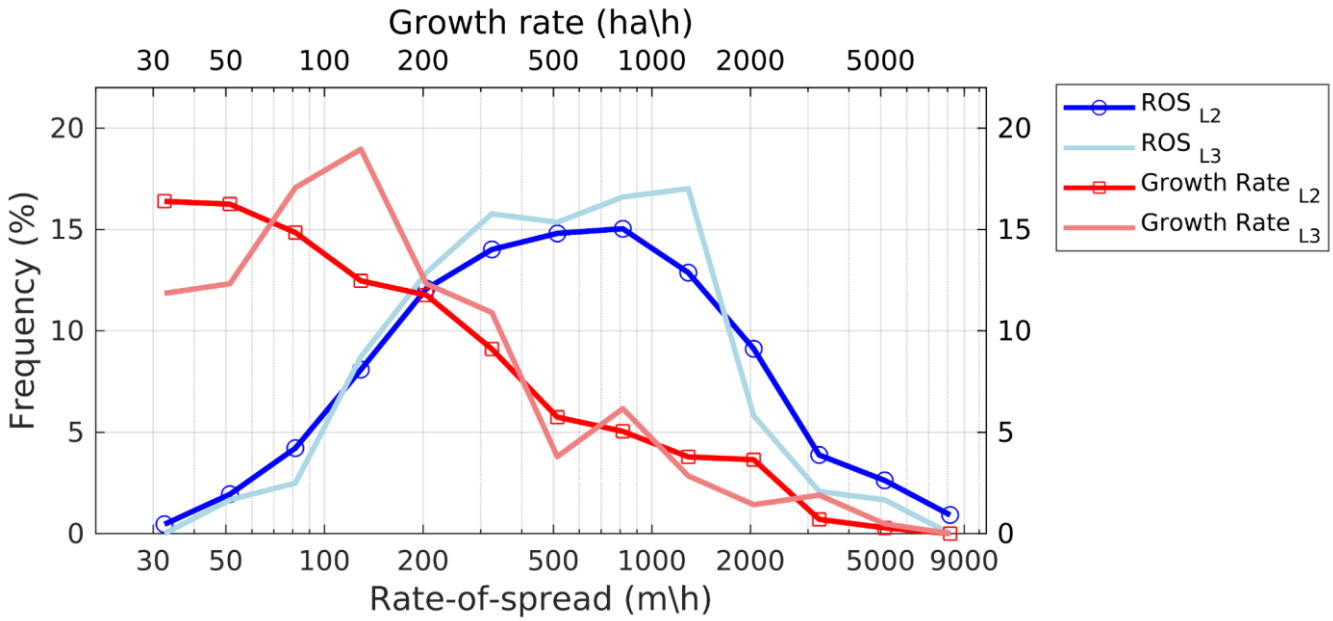

Figure 7: Estimated ROS and FGR distributions for L2 and L3 data (in log-scale). Each point represents the frequency in evenly spaced bins on a logarithmic scale.

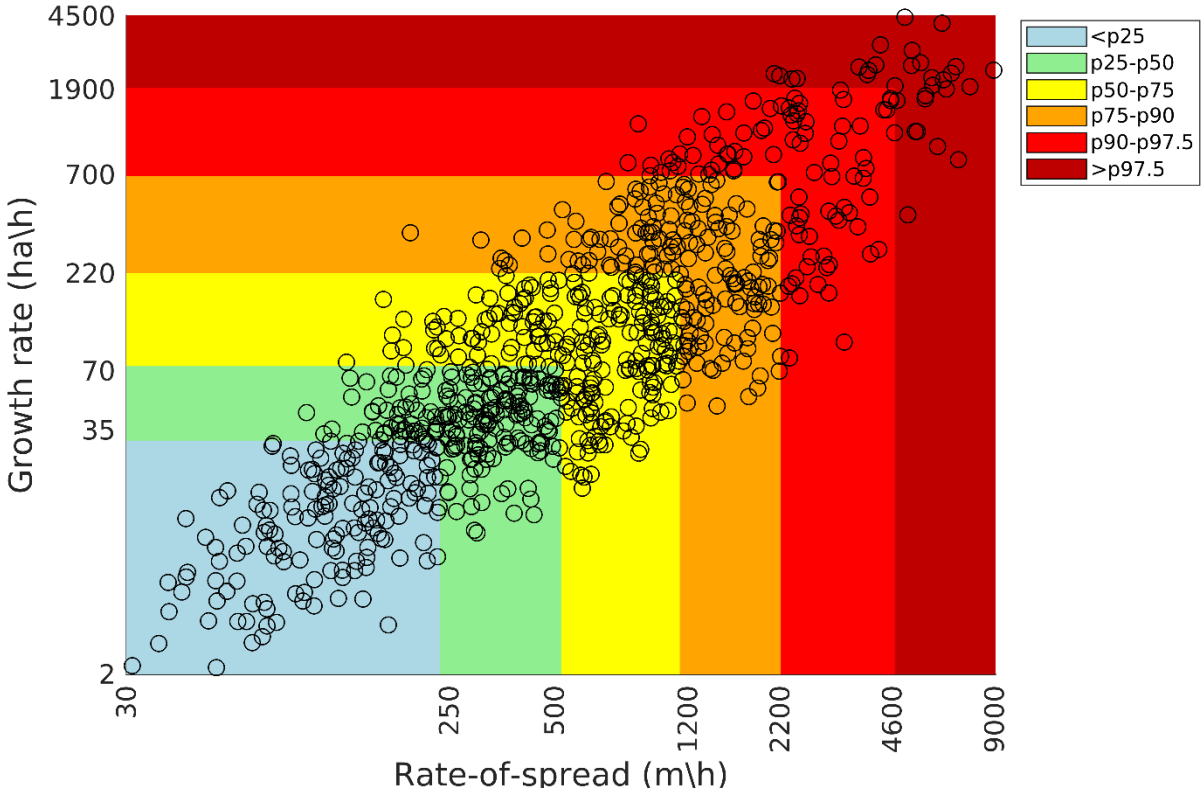

Figure 8: Distribution of the estimated partial rate-of-spread (ROSp) and FGR (L2). Each point represents a wildfire progression with at least 25 ha of extent. The percentiles were calculated for each variable separately (n=874). Colors represent percentile intervals for both fire behaviour descriptors.

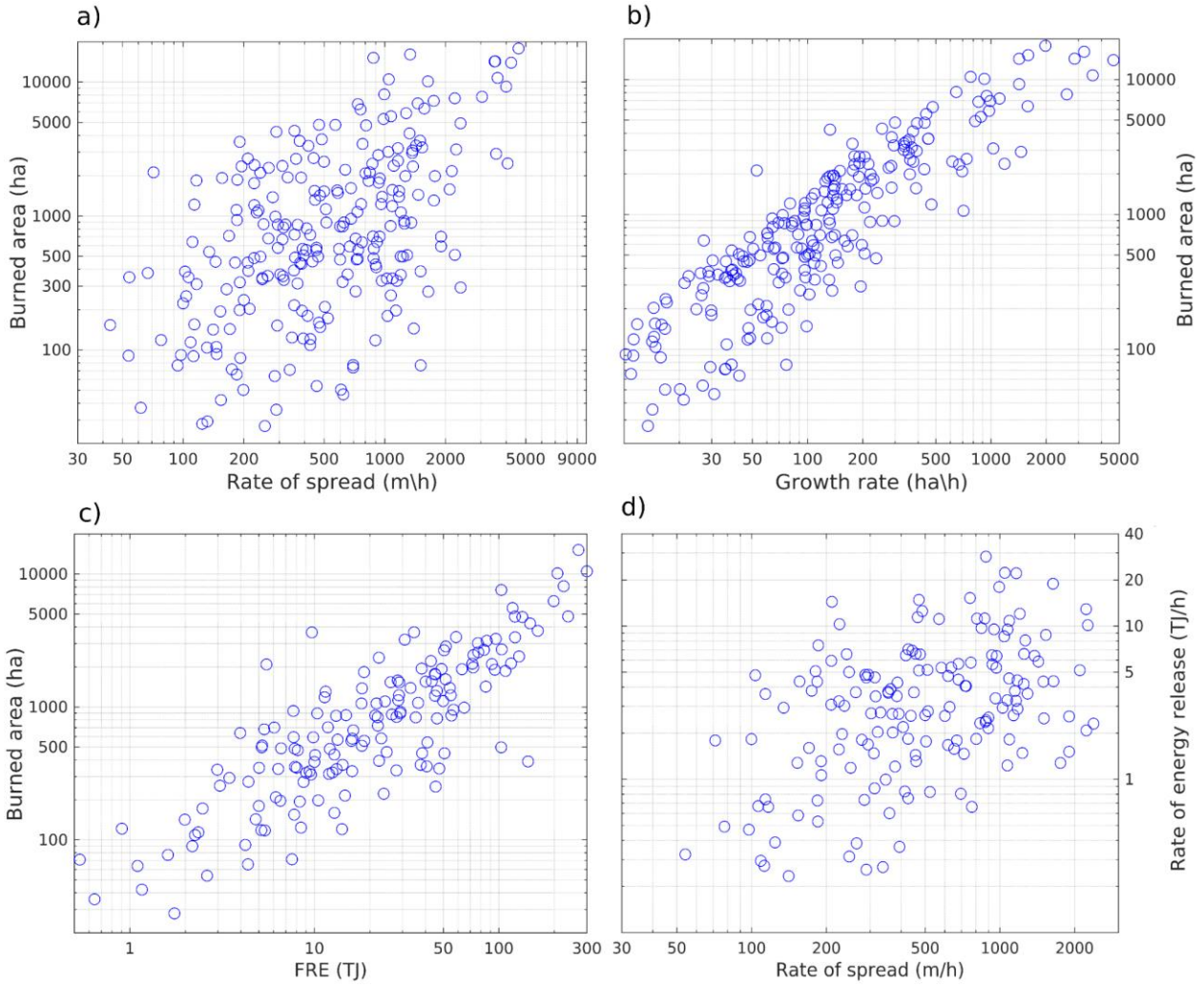

Figure 9: Comparison between simplified wildfire behaviour descriptors (L3): burned area extent and ROS (a), burned area extent and FGR (b), burned area extent and FRE (c), and ROS and average rate of energy release (d). The latter was calculated by dividing the total FRE by the burning period duration.

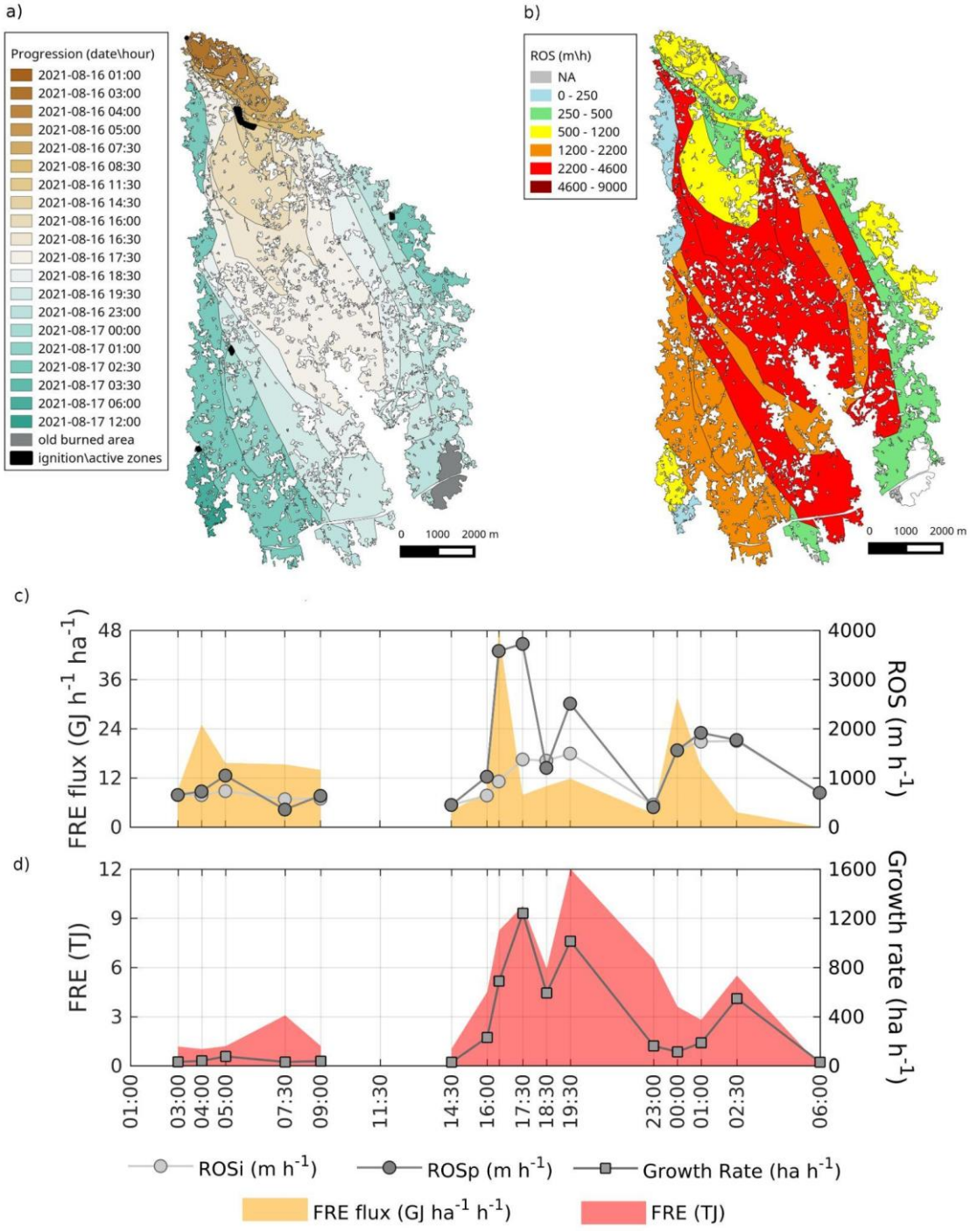

Figure 10: The Castro Marim (2021) wildfire progression (a). Wildfire behaviour descriptors include: the spatial distribution of ROS (b); the temporal distribution of ROS and FRE flux rate (c); and the temporal distribution of FRE and FGR (d). Plots (c) and (d) start at 01:00 of the 16th of August and end at 06:00 of the 17th of August.

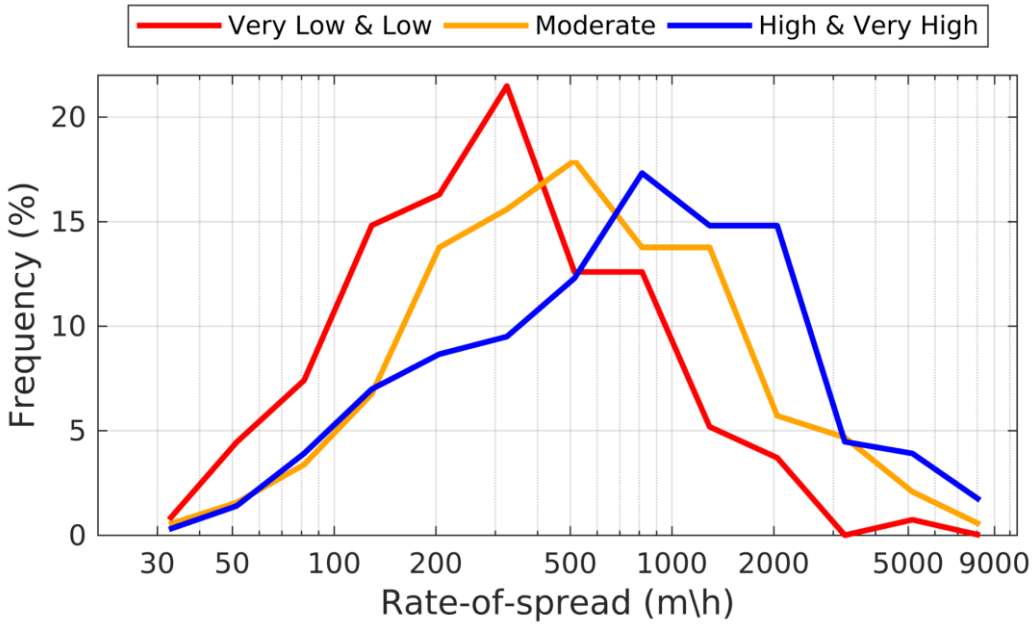

Figure B1: Histogram of the estimated ROS (L2) for three aggregated levels of confidence. L2 ROS estimates were used and the confidence flags are explained in Table A1.

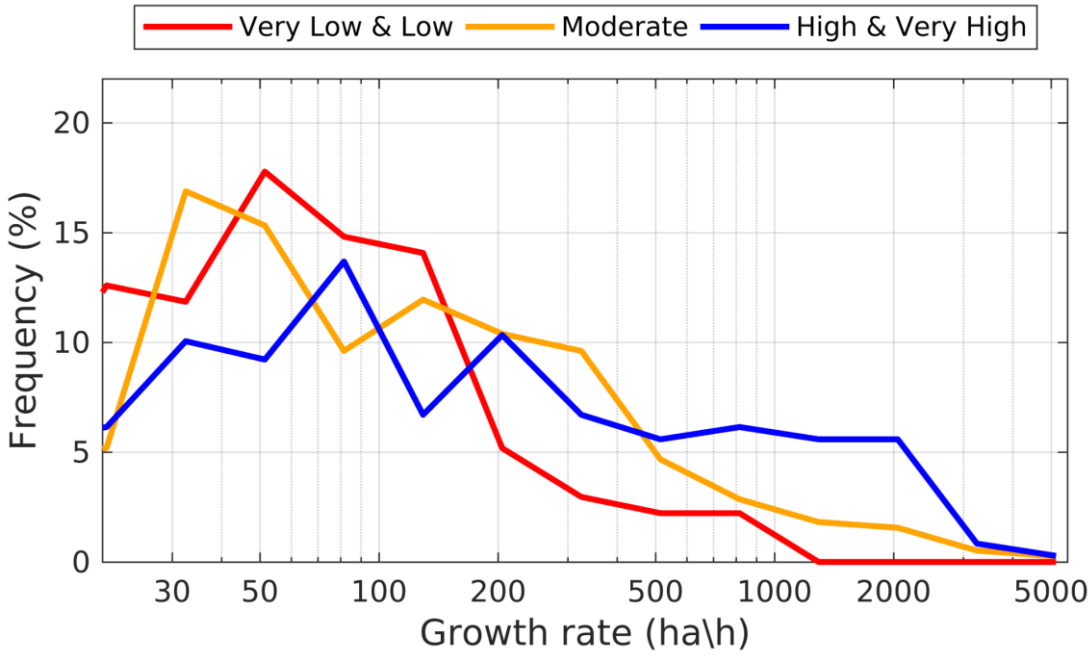

Figure B2: Histogram of the estimated FGR for three levels of confidence. L2 FGR estimates were used and the confidence flags are explained in Table A1.

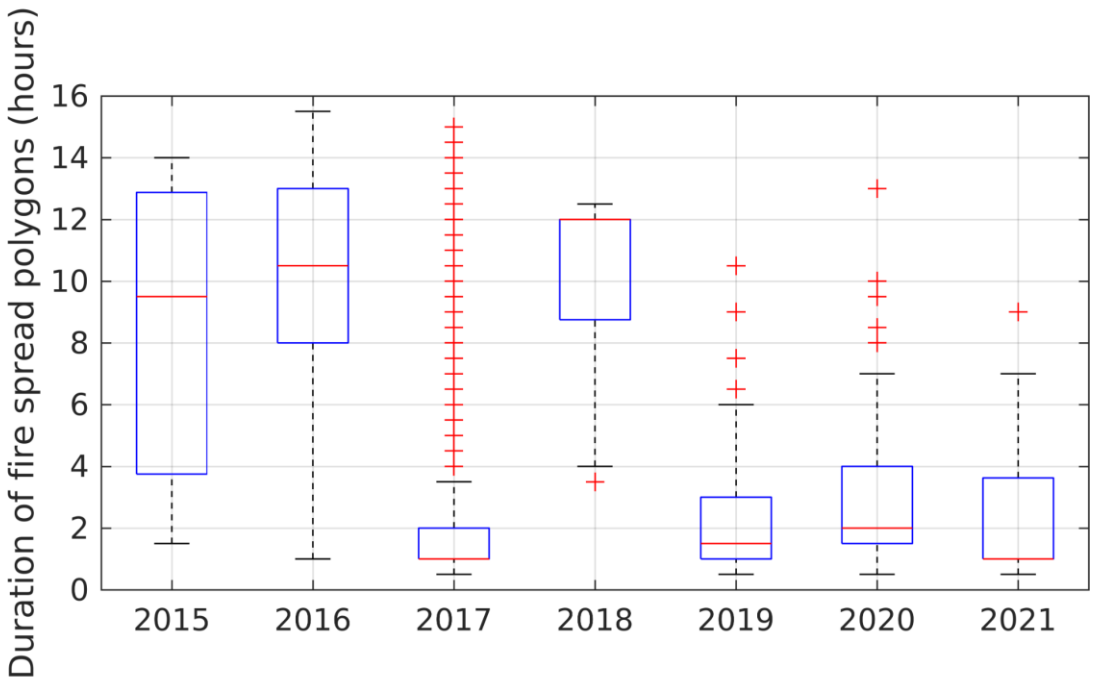

Figure B3: Distribution of the duration of the progression polygons divided by years

Tables

Table A1. Summary of major data sources and associated characteristics

Source	Description	Type of data	Temporal frequency	Spatial Resolution
Airborne	Initial-attack heli-brigades	Visible imagery	Depends on fire occurrence; up to the first 30min after wildfire alert	na
Airborne	Aeroplane	Visible, IR and thermal imagery and videos	Depends on fire occurrence; up to four flights per days	<1m*
Airborne	Coordination Helicopter	Visible images	Depends on fire occurrence	na
Satellite	Sentinel-2 (S2)	Visible and IR imagery	Every 5 days	10m – 60m
Satellite	Landsat 8/9	Visible and IR imagery	Every 5 days	30m
Satellite	PROBA_V	Visible and IR imagery	Daily** and every 5 days***	**300m; ***100m
Satellite	VIIRS NPP and NOAA-20	Visible and IR imagery	Up to 4 times per day	375m-750m
Satellite	VIIRS NPP and NOAA-20	Thermal anomalies	Up to 4 times per day	375m
Satellite	MODIS Terra and Aqua	Visible and IR imagery	Up to 4 times per day	250m-1000m
Satellite	MODIS Terra and Aqua	Thermal anomalies	Up to 4 times per day	1000m
Satellite	Sentinel 3	Visible and IR imagery	Twice per day (SLSTR), once per day (OLCI)	300-1000m
Satellite	MSG-SEVIRI	Thermal anomalies	Every 15 min	4000 m
Ground	Fire operatives	Visible imagery and videos	Depends on fire occurrence	na
Ground	Fire operatives	Georeferenced points and polygons	Depends on fire occurrence	na
Official fire data	Burned area	Perimeters	annual	na (derived from S2 imagery)
Official fire data	Ignition	Point	annual	na (derived from S2 imagery)
Official fire data	Time log	Report	Depends on fire occurrence	na
Reports of 2017 large wildfires	Guerreiro et al., (2017 and 2018)	Progression polygons	hourly	na

* depends on aeroplane flight height and on the sensor (visible sensors have higher resolution than IR sensors)

Table A2. Confidence flag value, class and interpretation. The flag is defined for each wildfire.

Flag value	Flag Class	Interpretation
1	Very Low	The major fire progressions were observed only with satellite data, with important associated uncertainties.
2	Low	The major fire progressions were observed only with satellite data with moderate uncertainties
3	Moderate	The major fire progressions were observed with satellite data with low/moderate uncertainties and complemented with other sources.
4	High	The major fire progressions were at least partially observed with ground and airborne data, with relevant uncertainties associated (e.g. the exact hour of an important progression, or a flank position, etc)
5	Very High	The major fire progressions were observed with ground and airborne data with low uncertainties

Table A3. Database metadata list for L1

ID	Fire Name	Municipality	Civil Parish	Start Date	End Date	Extent (ha)	Confidence flag	ANEPC incident ID	P1	P2
1	Gouveia_10082015	Gouveia	Mangualde da Serra	2015-08-10	2015-08-12	2513	2	2015090024014	99	86
2	Oleiros_03082015	Oleiros	Alvaro	2015-08-03	2015-08-04	853	2	2015050020535	100	95
3	VilaNovadeCerveira_08082015	Vila Nova de Cerveira	Candemil	2015-08-08	2015-08-09	2988	3	2015160019994	87	87
4	Agueda_08082016	Águeda	Préstimo	2016-08-08	2016-08-12	7317	1	2016010058351	99	63
5	Anadia_10082016	Anadia	V.N. de Monsarros	2016-08-10	2016-08-12	3370	2	2016010059055	97	80
6	ArcosdeValdevez_08082016	Arcos de Valdevez	Cabana Maior	2016-08-08	2016-08-11	5806	1	2016160022311	93	71
7	Arouca_08082016	Arouca	Janarde	2016-08-08	2016-08-14	23547	2	2016010058554	97	96
8	Boticas_05092016	Boticas	Codecoso	2016-09-05	2016-09-07	1694	3	2016170021732/ 2016170021835	97	97
9	CabeceirasdeBasto_06092016	Cabeceiras de Basto	Rio Douro	2016-09-06	2016-09-07	1336	2	2016030067614	100	100
10	Caminha_09082016	Caminha	Argela	2016-08-09	2016-08-11	1628	1	2016160022551	99	61
11	Cinfaes_07082016	Cinfães	Cinfães	2016-08-07	2016-08-08	567	1	2016180042605	95	95
12	Cinfaes_08082016	Cinfães	Oliveira do Douro	2016-08-08	2016-08-09	756	2	2016180042656	100	100
13	FreixodeEspadaaCinta_06092016	Freixo de Espada a Cinta	Freixo Espada à Cinta e Mazouco	2016-09-06	2016-09-07	5194	3	2016040027372	99	97
14	Moncao_06092016	Monção	Riba de Mouro	2016-09-06	2016-09-07	656	2	2016160025950	71	58
15	Moncao_09082016	Monção	Barroças e Taias	2016-08-09	2016-08-11	1115	1	2016160022460	77	77
16	ParedesdeCoura_07082016	Paredes de Coura	Meixedo	2016-08-07	2016-08-12	10457	2	2016160022456	100	96
17	PontedeLima_08082016	Ponte de Lima	Calheiros	2016-08-08	2016-08-09	739	1	2016160022390	91	75
18	SeverdoVouga_09082016	Sever do Vouga	Pessegueiro do Vouga	2016-08-10	2016-08-12	1818	3	2016010058973	96	94
19	VieiradoMinho_10082016	Vieira do Minho	Rossas	2016-08-10	2016-08-11	1637	2	2016030060428	99	96
20	Resende_17082017	Resende	S. Martinho de Mouros	2017-08-17	2017-08-21	544	1	2017180043566	84	38
21	RibeiradePena_15082017	Ribeira de Pena	Cerva	2017-08-15	2017-08-16	507	1	2017170021591	100	100
22	CastroDaire_05102017	Castro Daire	Almofala	2017-10-05	2017-10-05	701	2	2017180054022	99	99
23	Mortagua_07102017	Mortagua	Espinho	2017-10-07	2017-10-08	961	2	2017180054507	99	99
24	Mirandela_16072017	Mirandela	Alvites	2017-07-16	2017-07-17	949	2	2017040020105	100	88
25	Pombal_06102017	Pombal	Abiul	2017-10-06	2017-10-07	1225	2	2017100054724	100	100
26	TorredeMoncorvo_18072017	Torre de Moncorvo	Acoreira	2017-07-18	2017-07-18	1536	3	2017040020365	100	100
27	Guarda_23082017	Guarda	Fernão Joanes	2017-08-23	2017-08-25	3457	3	2017090026098	91	91
28	Serta_08092017	Serta	Pedrogao Pequeno	2017-09-08	2017-09-09	4177	3	2017050027511	100	100

29	Abrantes_09082017	Abrantes	Aldeia do Mato	2017-08-09	2017-08-10	4357	3	2017140045924	83	79
30	CasteloBranco_23072017	Castelo Branco	Santo André das Tojeiras	2017-07-23	2017-07-28	4569	3	2017050023219	97	85
31	Serta_15102017_2	Serta	Pedrógão Pequeno	2017-10-15	2017-10-16	2320	3	2017050030728	54	54
32	CasteloBranco_13082017	Castelo Branco	Louriçal do Campo	2017-08-13	2017-08-15	6173	2	2017050025136	100	96
33	PampilhosadaSerra_06102017	Pampilhosa da Serra	Fajao	2017-10-06	2017-10-09	7217	2	2017060044928	97	96
34	Guarda_17072017	Guarda	Rochoso	2017-07-17	2017-07-18	7523	2	2017090021641	88	88
35	FigueiradaFoz_15102017	Figueira da Foz	Quiaios	2017-10-15	2017-10-17	15141	4	2017060046330	100	97
36	Oleiros_23082017	Oleiros	Cambas	2017-08-23	2017-08-25	7985	3	2017050026111	88	67
37	Gois_17062017	Gois	Alvares	2017-06-17	2017-06-22	15852	3	2017060026571	100	99
38	Alcobaca_15102017	Alcobaca	Pataias	2017-10-15	2017-10-16	18575	4	2017100056537 /2017100056554	100	100
39	Arganil_15102017	Arganil	Coja	2017-10-15	2017-10-16	31970	3	2017060046312 /2017090031521	100	99
40	Serta_15102017	Serta	Figueiredo	2017-10-15	2017-10-17	30974	4	2017050030693	97	97
41	Alvaiazere_11082017	Alvaiazere	Pussos	2017-08-11	2017-08-19	23715	2	2017100043917/ 2017050025201	99	52
42	PedrogaoGrande_17062017	Pedrogao Grande	Pedrogao Grande	2017-06-17	2017-06-19	29456	4	2017100032538	92	91
43	Serta_23072017	Serta	Várzea dos Cavaleiros	2017-07-23	2017-07-27	33401	3	2017050023195	97	96
44	Lousa_15102017	Lousã	Vilarinho	2017-10-15	2017-10-17	45249	4	2017060046260	100	95
45	Agueda_15102017	Agueda	Albitelhe	2017-10-15	2017-10-16	9095	3	2017180056272	83	78
46	OliveiraFrades_15102017	OliveiraFrades	Varzielas	2017-10-15	2017-10-17	9297	3	2017180056290	99	97
47	Monchique_03082018	Monchique	Monchique	2018-08-03	2018-08-08	26227	3	2018080033743	93	82
48	Agueda_05092019	Agueda	Macinhata do Vouga	2019-09-05	2019-09-06	1602	3	2019010072794	89	84
49	Alijo_24072019	Alijo	Vila Verde	2019-07-24	2019-07-24	574	5	2019170019467	100	100
50	Baiao_04092019	Baião	Teixeira	2019-09-05	2019-09-06	728	3	2019130150620	75	73
51	Nisa_01082019	Nisa	Tolosa	2019-08-01	2019-08-01	712	5	2019120016787	99	98
52	Ourique_10062019	Ourique	Monte Lavarjao	2019-06-10	2019-06-10	554	5	2019020015472	75	75
53	Penedono_21072019	Penedono	Beselga	2019-07-21	2019-07-23	736	4	2019180039496	99	99
54	Sabugal_29082019	Sabugal	Vale Mourisco	2019-08-29	2019-08-29	578	5	2019090029579	100	100
55	Serta_13092019	Sertã	Marmeleiro	2019-09-13	2019-09-14	676	4	2019050028005	100	90
56	Tomar_03082019	Tomar	São Pedro Tomar	2019-08-03	2019-08-03	511	4	2019140045796	86	73
57	Valenca_04092019	Valença	Cerdal	2019-09-04	2019-09-05	642	1	2019160026115	83	83
58	Valpacos_13092019	Valpaços	Ervões	2019-09-13	2019-09-13	738	2	2019170026369	56	56
59	ViladeRei_20072019	Vila de Rei	Fundada	2019-07-20	2019-07-22	9305	3	2019050022178	99	99
60	MirandadoCorvo_13092019	Miranda do Corvo	Moinhos	2019-09-13	2019-09-14	540	3	2019060042282	96	96

61	Fundao_07082020	Fundão	Capinha	2020-08-07	2020-08-08	472	4	2020050018968	87	85
62	Silves_06072020	Silves	Boião	2020-07-06	2020-07-06	520	4	2020080025576	77	77
63	Avis_21072020	Avis	Montes Juntos	2020-07-21	2020-07-21	698	5	2020120014122	95	95
64	IdanhaaNova_30062020	Idanha-a-Nova	Salvaterra do Extremo	2020-06-30	2020-06-30	728	4	2020050015270	100	100
65	SaoJoaoPesqueira_10072020	São João da Pesqueira	Riodades	2020-07-10	2020-07-11	770	4	2020180031783	97	94
66	Fundao_06082020	Fundao	Bogas Baixo	2020-08-06	2020-08-06	749	5	2020050018872	96	96
67	PortoMos_06092020	Porto de Mós	Codacal	2020-09-06	2020-09-07	998	4	2020100046280	97	91
68	OliveiraFrades_07092020	Oliveira de Frades	Antelas	2020-09-07	2020-09-08	1902	3	2020180044235	86	73
69	Aljezur_19062020	Aljezur	Bordeira	2020-06-19	2020-06-20	2243	5	2020080023014	99	93
70	Sernancelhe_06082020	Sernancelhe	Lapa	2020-08-06	2020-08-06	2213	5	2020180037681	100	100
71	Chaves_30072020	Chaves	Vila Verde da Raia	2020-07-30	2020-07-31	2508	3	2020170018342	83	82
72	Oleiros_25072020	Oleiros	Sardeiras de Baixo	2020-07-25	2020-07-27	5564	3	2020050017687	95	92
73	ProencaaNova_13092020	Proenca-a-Nova	Cunqueiros	2020-09-13	2020-09-14	14568	4	2020050022403	91	91
74	CasteloBranco_29082020	Castelo Branco	Ponsul	2020-08-29	2020-08-29	315	4	2020050021105	100	92
75	CastroDaire_07092020	Castro Daire	Cujo	2020-09-07	2020-09-07	452	4	2020180044155	76	76
76	Odemira_18082021	Odemira	João Martins	2021-08-18	2021-08-19	944	5	2021020019189	100	98
77	CastroMarim_16082021	Castro Marim	Pernadeira	2021-08-16	2021-08-17	5956	5	2021080035488	100	99
78	Monchique_17072021	Monchique	Tojeiro	2021-07-17	2021-07-18	1900	4	2021080029244	99	99
79	FreixoEspadaaCinta_20082021	Freixo de Espada à Cinta	Lagoaça	2021-08-20	2021-08-20	412	4	2021040023667	71	71
80	Mogadouro_20072021	Mogadouro	Tó	2021-07-20	2021-07-20	253	5	2021040019425	99	98

p1: stands for percentage of known fire progression (%); p2: stands for percentage fire behaviour descriptors calculated (%)

Table A4. Attribute fields of the fire progressions (L1)

Field	Description	Possible values
id	Polygon ID	>0
type	Type of Spread Polygon	p - wildfire progression ; z - ignition or active flaming zone ; a - previously burned area
date_hour	Date and hour of the polygon	yyyy-mm-dd hh:mm; uncertain ; na (not applicable)
source	Source of the data	fserv - forest service ; sat - satellite data ; airb - airborne data; fops - fire personnel; ek - expert knowledge; rep - external reports
zp_link	Numerical link between a ignition or active flaming zone (“z”) polygon and a wildfire progression (“p”) polygon	1,2,3... - the link between types "p" and "z" with known dates and hours; 0 - used for type "a" or when progression in "uncertain" or when the link between "p" and "z" is unknown
burn_period	Burning period	1,2,3,..; 0 for the same cases as “zp_link”.

Table A5. Attribute fields of the fire behaviour database (L2)

Field	Description	Possible values
fid	Fire ID	1-80*
fname	Fire Name	Municipality_StartDate (e.g. Gouveia_10082015)
year	Year	2015-2021*
type	Type of Spread Polygon	p - wildfire progression ; z - ignition or active flaming zone ; a - previously burned area
sdate	Start date and hour of the polygon	yyyy-mm-dd hh:mm; uncertain ; na (not applicable)
edate	End date and hour of the polygon	yyyy-mm-dd hh:mm; uncertain ; na (not applicable)
inidoy	Start day-of-year of the polygon (hours in decimal values)	1 to 366; -1 for uncertain progression polygons, polygons with unknown zp_link and previously burned areas
enddoy	End day-of-year of the polygon (hours in decimal values)	1 to 366; -1 for uncertain progression polygons, polygons with unknown zp_link and previously burned areas
source	Source of the data	fserv - forest service ; sat - satellite data ; airb - airborne data; fops - fire personnel; ek - expert knowledge; rep - external reports
zp_link	Numerical link between a ignition or active flaming zone (“z”) polygon and a wildfire progression (“p”) polygon	1,2,3... - the link between types "p" and "z" with known dates and hours; 0 - used for type "a" or when progression in "uncertain" or when the link between "p" and "z" is unknown
burn_period	Burning period	1,2,3,..; 0 for the same cases as “zp_link”.
area	Burned area extent (ha)	> 0 for progression polygons, -1 for ignition or active flaming zones.
growth_rate	Fire growth rate (ha/h)	>0 for progression polygons with zp_link value >0; -1 for previously burned areas or uncertain progression polygons
ros_i	Average rate-of-spread (m/h) calculated since ignition\active flaming areas or a progression marking the start of the burning period	>0 for progression polygons with zp_link value >0; -1 for previously burned areas or uncertain progression polygons
ros_p	Parcial rate-of-spread (m/h) calculated between consecutive ignition\active flaming areas and progression polygon, or between two consecutive progression polygons	>0 for progression polygons with zp_link value >0; -1 for previously burned areas or uncertain progression polygons
spdir_i	Spread direction associated with “ros_i” (° from North)	0 to 359.99; -1 for the same cases in “ros_i”
spdir_p	Spread direction associated with “ros_p” (° from North)	0 to 359.99; -1 for the same cases in “ros_p”

duration_i	Duration (hours) associated with the “ros_i” metric	>0 known progression polygons; -1 for ignition\active flaming zones, previously burned áreas or uncertain progression polygons
duration_p	Duration (hours) associated with the “ros_p” metric	>0 known progression polygons; -1 for ignition\active flaming zones, previously burned áreas or uncertain progression polygons
qc	Confidence flag for each wildfire	See table A1
FRE	Fire Radiative Energy (TJ)	>0 for known progressions with at least 70% of FRE observations between “sdate” and “edate”; - 1 for the remaining polygons
FRE_flux	Fire Radiative Energy flux (TJ ha^{-1} h^{-1})	>0 for known progressions with at least 70% of FRE observations between “sdate” and “edate”; - 1 for the remaining polygons
FRE_perc	Percentage of FRE observations between “sdate” and “edate”	Between 0 and 100 for known progression polygons; -1 for the remaining.

* values will change when the database will be updated with new wildfires.

Table A6. Attribute fields of the simplified fire behaviour database (L3)

Field	Description	Possible values
fid	Fire ID	1-80*
fname	Fire Name	Municipality_StartDate (e.g. Gouveia_10082015)
burn_period	Burning period	⩾1
year	Year	2015-2021*
sdate	Start date and hour of the burning period	yyyy-mm-dd hh:mm; "na" for burning periods which only have progression polygons with unknown "zp_link" (see Table A4)
edate	End date and hour of the burning period	yyyy-mm-dd hh:mm; "na" for burning periods which only have progression polygons with unknown "zp_link" (see Table A4)
inidoy	Start day-of-year of the burning period (hours in decimal values)	1 to 366; -1 for burning periods which only have progression polygons with unknown "zp_link" (see Table A4)
enddoy	End day-of-year of the burning period (hours in decimal values)	1 to 366; -1 for burning periods which only have progression polygons with unknown "zp_link" (see Table A4)
qc	Confidence flag for each wildfire	See table A1
area	Burned area extent (ha)	>0
growth_rate	Average fire growth rate (ha/h)	>0; -1 for burning periods which only have progression polygons with unknown "zp_link" (see Table A4)
ros	Average rate-of-spread (m/h)	>0; -1 for burning periods which only have progression polygons with unknown "zp_link" (see Table A4)
max_ros	Maximum rate-of-spread (m/h) observed in the burning period	>0; -1 for burning periods which only have progression polygons with unknown "zp_link" (see Table A4)
spdir	Spread direction associated with "ros_i" (° from North)	0 to 359.99; -1 for burning periods which only have progression polygons with unknown "zp_link" (see Table A4)
duration	Duration (hours) of the burning period	>0; -1 for burning periods which only have progression polygons with unknown "zp_link" (see Table A4)
FRE	Fire Radiative Energy (TJ)	>0 for known progressions with at least 70% of the area burned during the burning period covered with FRE estimates; - 1 for the remaining polygons
FRE_flux	Fire Radiative Energy flux (TJ ha^{-1} h^{-1})	>0 for known progressions with at least 70% of the area burned during the burning period covered with FRE estimates; - 1 for the remaining polygons
FRE_perc	Percentage of FRE observations between "sdate" and "edate"	Between 0 and 100

* values will change when the database will be updated with new wildfires.